OBSERVATION AND TRACKING OF TROPICAL CYCLONES

USING RESOLUTION ENHANCED SCATTEROMETRY

by

R. Ryan Halterman

A thesis submitted to the faculty of

Brigham Young University

in partial fulfillment of the requirements for the degree of

Master of Science

Department of Electrical and Computer Engineering

Brigham Young University

October 2006

BRIGHAM YOUNG UNIVERSITY

GRADUATE COMMITTEE APPROVAL

of a thesis submitted by

R. Ryan Halterman

This thesis has been read by each member of the following graduate committee and by majority vote has been found to be satisfactory.

_____   _____
Date   David G. Long, Chair

_____   _____
Date   Karl F. Warnick

_____   _____
Date   D. J. Lee

ABSTRACT

OBSERVATION AND TRACKING OF TROPICAL CYCLONES USING

RESOLUTION ENHANCED SCATTEROMETRY

R. Ryan Halterman

Department of Electrical and Computer Engineering

Master of Science

The QuikSCAT scatterometer provides global daily coverage of oceanic near-surface vector winds. Recently, algorithms have been developed to enhance the spatial resolution of QuikSCAT winds from 25 km to 2.5 km posting. These ultra-high resolution winds are used, in comparison with standard L2B data product winds, to observe and track tropical cyclones.

Resolution enhanced winds are found to provide additional storm structure such as inner core size and structure and the presence of multiple eyewalls compared with standard resolution winds. The 2.5 km winds are also able to observe storms nearer to the shore than 25 km winds.

An analysis of circulation center locatability with each resolution wind field is performed. Center fixes with enhanced resolution winds are nearer the National Hurricane Center best-track positions than are standard resolution center fixes. A data and image set of every tropical cyclone worldwide observed by Seawinds on QuikSCAT or SeaWinds on ADEOS II from 1999 through 2003 is generated and made available to the scientific community at http://scp.byu.edu.

ACKNOWLEDGMENTS

I would like to thank Dr. David Long for his patience, guidance, instruction, and friendship. His example will long be with me. I would also like to acknowledge the influence of my parents, and especially my grandfather, in my love for learning. Finally, I would like to thank Julie for her boundless love and encouragement and Sam for keeping a smile on my face.

Contents

List of Tables

List of Figures

xviii

Chapter 1

Introduction

One of the most disruptive of natural disasters, tropical cyclones have long garnered significant attention from the scientific community. Early meteorologists were limited in their tropical cyclone observations to near coastal and sporadic ship-based measurements. Beginning in 1945 with the 53rd Weather Reconnaissance Squadron, aerial observation of hurricanes became possible. Then, with the launch of the first weather satellites, in the 1950s and 1960s, scientists gained further tropical cylone observation ability. Space-borne remote sensing has enabled much improvement in tropical cyclone understanding and prediction. This thesis focuses on the observation of tropical cyclones by wind scatterometers—a class of space-borne remote sensors.

Wind scatterometers are differentiated from other radars by their highly-calibrated measurements of the returned pulse power from multiple azimuth angles. The pulse power backscattered by a distributed target such as the Earth's surface contains information about its roughness and dielectric properties. Surface roughness is generally direction dependent. Thus, multiple azimuth observations are required to fully characterize it. From the surface roughness at a variety of observation geometries, the near-surface ocean wind speed and direction can be inferred. Space-borne scatterometers can observe a large portion of the Earth's surface daily, and can measure surface backscatter and infer surface winds in nearly all weather conditions and regardless of solar illumination. Satellites are also able to observe areas that would otherwise be prohibitively costly or dangerous. This is a great boon to meteorologists interested in the wind structure of tropical cyclones which often occur far out at sea and in dangerous environments.

1.1 Importance of Monitoring Tropical Cyclones

In addition to the readily apparent effects to life and infrastructure, tropical cyclones serve as a significant mechanism for global heat dissipation. They may also act as a forebear to other climate conditions such as warming by greenhouse gases. Some scientists believe that an increase in sea surface temperatures brought on by greenhouse warming will be correlated with a statistical trend of increased tropical cyclone intensity. Frequent and accurate tropical cyclone observation from genesis to dissipation is important in understanding their role in Earth's climate. A better understanding of the processes involved in tropical cyclones is also requisite for improvements in track and intensity forecasting.

Technological developments over the past few decades have enabled a significant increase in the accuracy of storm track forecasting. These advances were brought about by research that led to a better understanding of tropical cyclones' interaction with large-scale steering currents.

Storm intensity forecasting, however, has not seen comparable gains. Among the impediments to improved intensity forecasting is an incomplete understanding of the complexities of intensification. Advances in intensity forecasting will require a better understanding of tropical cyclone processes occurring on a much smaller scale than those affecting track forecasting. Increased understanding and modeling of physical and dynamic processes affecting the inner core structure and its interaction with the surrounding environment are paramount. Ongoing studies into these complexities are facilitated by frequent and accurate monitoring of the related parameters at sufficient resolution.

1.2 Description of the Problem

Modern advances enable researchers to monitor tropical cyclones in a variety of ways. *In situ* observation remains important for the most accurate measurements of atmospheric pressure, wind speed and direction, and other parameters, but sufficient aerial reconnaissance of tropical cyclones on a global scale is prohibitively costly and dangerous. Surface-based measurement by ship and buoy is used, but is inadequate

for storm-scale observation because of its sparse and sporadic sampling. Space-borne observation using visible and infra-red sensors, microwave radiometers, precipitation radars, and scatterometers contribute to a greater understanding of tropical cyclone conditions. They do so over expansive scales and without endangering *in situ* data collectors.

The National Hurricane Center (NHC)—part of the National Oceanic and Atmospheric Administration (NOAA)—in Miami, Florida is the U.S. agency responsible for tropical cyclone prediction and monitoring over the Eastern Pacific and the Atlantic. In other storm basins, the Joint Typhoon Warning Center (JTWC)—a U.S. Department of Defense agency—in Pearl Harbor, Hawaii fills this role. To fulfill their missions, the NHC and JTWC employ all of the above data sources. Among the difficulties facing those desiring to improve tropical cyclone genesis, track, and intensity forecasting are accurate and timely high-resolution estimates of the wind field—both speed and direction—of the storm.

Launched in 19 June 1999, the SeaWinds scatterometer aboard QuikSCAT was designed to provide accurate, near global daily coverage of ocean surface winds. It is still operating, well beyond its projected 3-year mission life. A nearly identical follow-on, launched aboard the Advanced Earth Observing Satellite 2 (ADEOS II) on 14 December 2002, had an unfortunately short mission life ending on 24 October 2003 due to solar power failure. The winds retrieved by the SeaWinds scatterometers are highly accurate within a range of moderate wind speeds and in limited rain. At extreme wind speeds and in intensely raining conditions, their absolute accuracies degrade somewhat. Within this thesis the term QuikSCAT will generally refer to both sensors collectively.

Notwithstanding the diminished accuracy in conditions typifying hurricanes, QuikSCAT has proven useful to tropical cyclone forecasters. QuikSCAT winds have been assimilated into operational data for the National Oceanic and Atmospheric Administration's (NOAA) Ocean Prediction Center (OPC) and have proven valuable [1]. It is also favorably impacting early detection of tropical cyclones [2], numerical weather prediction [3], and other scientific applications [4]. Recently, methods

have been developed to increase the resolution of QuikSCAT wind fields from 25 km to 2.5 km posting [5]. The dramatically increased resolution permits a more detailed examination of wind field structure of tropical cyclones at the expense of potential noise within the wind field—especially the wind direction field. This thesis explores the relative utility of these resolution enhanced QuikSCAT winds for tropical cyclone observation.

1.3   Thesis Outline

This thesis is organized into five chapters with one appendix. Chapter 2 provides background on tropical cyclones and cyclogenesis. A brief history of scatterometry is given. It also presents background on the SeaWinds scatterometer and scatterometry theory—including resolution enhancement.

Chapter 3 is a summary look at tropical cyclone wind field retrievals. The QuikSCAT-derived wind field images are evaluated for their usefulness in observing tropical cyclone parameters of interest. A variety of inner core size and structure, concentric eyewall, near-land observation, and ambiguous circulation center conditions are explored.

Chapter 4 compares the use of standard and enhanced resolution QuikSCAT wind fields for tropical cyclone center identification. A comprehensive data set of every tropical cyclone observed over the ocean by SeaWinds on QuikSCAT and SeaWinds on ADEOS II is created. To evaluate the relative utility of standard and enhanced resolution wind fields, center locations derived from images at each resolution are compared with National Hurricane Center best-track storm positions. Ultra-high resolution wind fields generally enable more accurate position fixes and with greater subjective confidence.

Chapter 5 concludes the body of this thesis by summarizing results and contributions, and describing future avenues of research. Appendix A supplements the main body with additional information on the automated tropical cyclone data set generation tools created for this study.

Chapter 2

Background

Spaceborne remote sensors have greatly increased in number and capability in recent years. They have also seen a commensurate increase in use and utility for monitoring tropical cyclones. This chapter provides basic background on tropical cyclones, cyclogenesis, and observation of tropical cyclones, and an overview of scatterometry algorithms for standard and enhanced resolution wind field retrieval.

2.1 Tropical Cyclones

The term *tropical cyclone* encompasses a wide variety of storms. It describes the weather system's formation in the tropics and the nature of wind circulation within the system—counter-clockwise in the northern hemisphere and clockwise in the southern. Specifically, a tropical cyclone is a warm-core, synoptic-scale cyclone with organized convection and closed circulation of surface winds about a well defined center [6].

Precise sub-terms for tropical cyclones vary by the storm's intensity and location. For weaker storms, all basins use the same referencing scheme: *tropical depression* for storms with winds less than 33 kt (17 m/s) and *tropical storm* for storms with winds between 33–63 kt (17–32 m/s). For more intense tropical cyclones, referencing terms vary by basin. Figure 2.1 diagrams the five principal basins of tropical cyclone formation monitored by US agencies. The National Hurricane Center (NHC) is tasked with storms originating in the Northern Atlantic (Region 1 in Fig. 2.1) and Eastern Pacific (Region 2). In these basins, tropical cyclones with winds exceeding 63 kt (32 m/s) are termed *hurricanes* after the Carib god of evil, Hurican. The
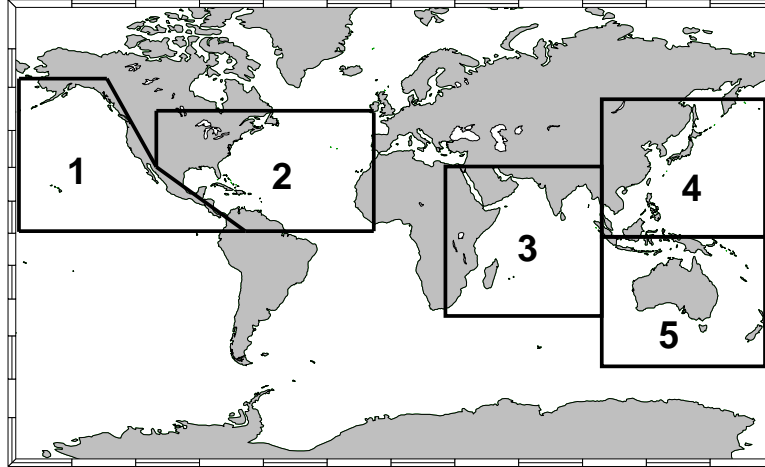
Figure 2.1: Map of tropical cyclone basins. 1) Eastern Pacific, 2) Northern Atlantic 3) Indian Ocean, 4) Western Pacific, and 5) Southern Pacific

Joint Typhoon Warning Center (JTWC) monitors tropical cyclones for US interests in the Indian Ocean (Region 3), Western Pacific (Region 4), and Southern Pacific (Region 5). Within these basins, the JTWC designates storms exceeding 63 kt (32 m/s) as *typhoons*. This term is thought to originate from a Cantonese phrase meaning "big wind". Other local agencies monitor these basins for their respective nations, but all reference data used herein is acquired from the NHC and JTWC.

Hurricanes are further classified according to maximum sustained winds (1 min. average) by the Saffir-Simpson Hurricane Scale, see Table 2.1. This scale attempts to estimate the expected damage to man-made structures from impacting storms. It originated in 1969 with Herbert Saffir, a civil engineer on commission by the United Nations to study low cost housing in hurricane prone areas. Bob Simpson, then director of the NHC, added expected storm surge values to the scale. Because classification is based on wind speeds alone, actual values of storm surge and resultant damage may vary widely due to related complexities. Other scales are used by local agencies to classify intense tropical cyclones in basins outside the Northern Atlantic and Eastern Pacific.

Table 2.1: Saffir-Simpson Hurricane Scale

Category (Damage)	Wind Speed	Storm Surge
1 (Minimal)	64–82 kt (33–42 m/s)	4–5 ft (1.2–1.5 m)
2 (Moderate)	83–95 kt (43–49 m/s)	6–8 ft (1.8–2.4 m)
3 (Extensive)	96–113 kt (50–58 m/s)	9–12 ft (2.7–3.7 m)
4 (Extreme)	114–135 kt (59–69 m/s)	13–18 ft (4.0–5.5 m)
5 (Catastrophic)	>135 kt (>69 m/s)	>18 ft (>5.5 m)

2.1.1 Tropical cyclogenesis

Though not fully understood, six conditions are generally necessary for tropical cyclone formation—or tropical cyclogenesis: pre-existing atmospheric disturbance, warm ocean waters, high humidity, sufficient atmospheric vertical temperature gradient, adequate distance from the equator, and weak vertical wind shear [7].

Tropical cyclones do not spontaneously develop. They require pre-existing disturbances with near-surface circulation. Cyclones may then intensify as the manifestation of a positive feedback heat engine. They are fueled by warmth—requisite water temperatures above 26°C (79°F)—and an essentially limitless supply of moisture from the ocean surface.

To permit the release of latent heat energy and fuel the tropical cyclone, the upper atmosphere must be sufficiently cool with respect to the rising warm moist air. The resultant saturation of the cool upper atmosphere contributes to the generation of cumulonimbus clouds which are effective transporters of additional heat and moisture to the upper atmosphere. Vertical transportation of warm air ceases at the tropopause so rising air spreads out laterally once reaching this boundary. This dissipation of the vertical air column further lowers near-surface pressures at the storm core and enhances surface wind convergence.

Cyclonic circulation is initiated by the Coriolis effect. For the force to be sufficiently strong, the emergent storm must occur at least 4°–5° (about 500 km) poleward. This cyclonic circulation further enhances wind convergence and the continued transportation of warm air to the storm's core.

In order for continued intensification, adequate linkage between the lower and
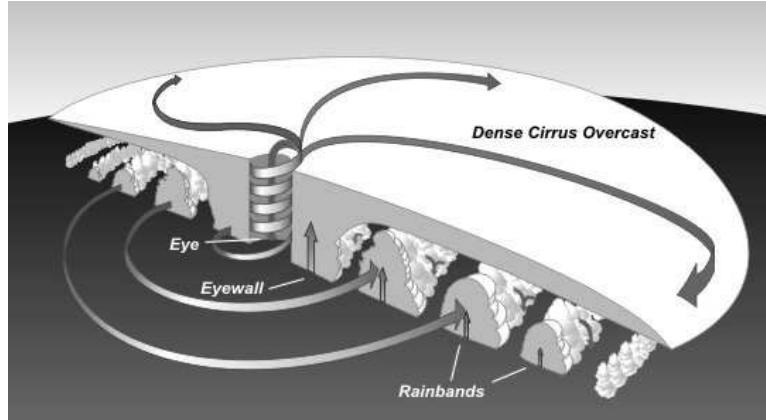
Figure 2.2: Tropical cyclone structure (NOAA) [8]

upper troposphere must exist so that mass can be transported vertically and then dispersed horizontally. A potentially disruptive force in this linkage is the presence of strong vertical wind shear. In the Southern Atlantic basin, excessive wind shear is one of the primary factors in the absence of tropical cyclones. Wind shear—a difference in wind speed or direction—in excess of about 15 kt (8 m/s) prohibits the necessary structure for appropriate heat dissipation and mass dispersion. Without these two elements, the storm is unable to maintain a sufficiently low central pressure for cyclonic wind convergence.

It should be noted that the above conditions are necessary, but not sufficient, for tropical cyclone formation and intensification. Frequently, all of the conditions appear to be met for cyclogenesis, yet the storm fails to materialize. This is one of the complications in tropical cyclone intensity forecasting.

2.1.2 Tropical cyclone structure

Upon formation and intensification, tropical cyclones exhibit a characteristic structure. Some of these features are diagrammed in Fig. 2.2. All strong tropical cyclones consist of a central area of low near-surface pressure. Above this low pressure area, a central warm core resides. Because of the vertical transportation of warm air at the storm's core, at any given altitude above the surface the air temperature in the core is warmer than its surroundings.

8

Above and surrounding the warm core, a shield of dense cirrus clouds make up the "central dense overcast" (CDO). As wind speeds within the storm's core increase, the center of the CDO breaks up frequently leaving a clear eye. Tropical cyclone eyes are thought to form because of interplay between conservation of angular momentum and inertia. Conservation of angular momentum requires that convergent winds move faster near the center of rotation. However, as the winds accelerate, they also experience inertial effects manifested as a centrifugal force. At about 64 kt (33 m/s), the threshold for hurricane classification, the spiraling winds cease to reach the center of the low pressure, but blow tangentially to lines of constant pressure a distance away. The absence of moist inflow at the very center of circulation impedes continued cloud formation in this region and the CDO dissipates revealing the recognizable eye.

Just outside the eye is generally found the most severe weather within the tropical cyclone. This region, called the eyewall, corresponds to the minimum radius of circulation for inward spiraling winds. It is typically the region of strongest winds.

The spiraling in of moist airflow at low levels results in the formation of cumulonimbus spiral bands—also known as rain or feeder bands—outside of the eyewall. As the moist influx creates cumulus clouds, they enhance the conditions for further cumulus formation and progression to cumulonimbus. This positive feedback between enhanced local convergence and cumulonimbus generation in the inflow perpetuates the feeder bands. The rain bands tend to rotate cyclonically inward at a speed slower than the prevailing wind.

At the upper elevations of a tropical cyclone, due to an increase in temperature and an influx of mass, high pressures develop. In response to the higher pressure, air begins to flow outward. The Coriolis effect causes the high-elevation outward-flowing air to spiral anti-cyclonically as it disperses the accumulated mass. This outflow is important as without it, central surface pressures would rise and weaken or potentially destroy the tropical cyclone.

Tropical cyclone motion results because of the larger scale air movement, called the steering current. In general, the steering current induces a forward speed on the order of 13 kt (7 m/s) for storms near the Equator. As the storm progresses, a
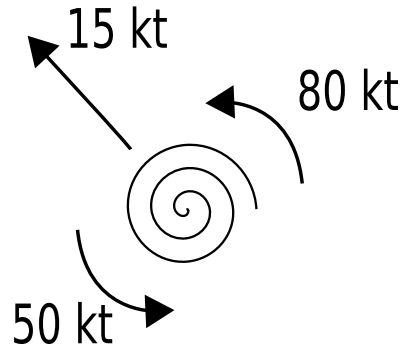
Figure 2.3: Asymmetric tropical cyclone speeds.

Coriolis acceleration deflects the storm pole-ward in the absence of counteracting forces. Storms moving pole-ward often increase in translational speed, sometimes to as fast as 50 kt (25 m/s).

Because of the additive effect of the tropical cyclone wind speed and the steering current (or forward speed), the wind speed distribution is often asymmetric. In Fig. 2.3, the stylized tropical cyclone has a nominal rotational wind speed of 65 kt. The vector addition of the 15 kt forward speed enhances wind components in the direction of travel and diminishes components in the opposite direction. Tropical cyclones in the northern hemisphere often exhibit higher wind speeds to the right of the forward track and lower speeds to the left. This phenomenon is reversed for southern hemisphere storms. Storm surges and property damages are often equally asymmetric.

2.1.3 Observation of tropical cyclones

Historically, observation of tropical cyclones has posed particular challenges. Surface level observations from weather stations are generally only available near coastal areas or from ships venturing into their path. Even in these cases, most useful observations are toward the storm exterior where conditions are less violent and do not damage the sensing platform. As such, it is difficult to obtain a full picture of tropical cyclones from surface measurements alone.

Reconnaissance flights into tropical cyclones have recently become possible,

however. Large, specially-equipped cargo planes—WC-130 Hercules and WP-3D Orions—are able to penetrate into the center of even intense storms. From there, a number of direct and remote sensing instruments are used to measure temperature, pressure, humidity, and wind speed. Among the available on-board sensors are flight level instruments, weather radars, and GPS dropsondes.

The latter of these, GPS dropsondes, provide a storm profile from flight level to the surface. Each of up to four simultaneous sondes parachutes to Earth while relaying temperature, pressure, humidity, and wind speed and direction back to the plane. Measurements of winds are achieved by using GPS derived positions to calculate the wind speed and direction causing the sonde to deviate from a vertical path.

Storms near land in many areas are observed by Doppler weather radars. Excellent storm characterizations are available from their high temporal and spatial resolution. At sea and in most basins, however, neither surface-based Doppler radars nor reconnaissance flights are available. In such cases, space-borne observation fills the gap. Optical and infrared data from geostationary satellites, and microwave radar and radiometer data from polar orbiting satellites all contribute to better observation and tracking of tropical cyclones.

2.2 Scatterometry

Amongst the space-borne sensors used to monitor tropical cyclones are scatterometers, a type of radar designed to measure near-surface ocean wind speed and direction. They can achieve near global daily coverage because of their generally polar orbit and wide swath width and are able to do so regardless of solar illumination and cloud cover.

Winds traveling over the ocean surface impart momentum to the ocean surface because of frictional forces. This momentum transfer induces small waves, called capillary waves, onto the surface. The amplitude and direction of these capillary waves is directly related to the wind speed and direction. This relation is exploited by scatterometers for wind retrieval.

11

2.2.1 The Geophysical Model Function

Scatterometers illuminate the ocean surface with electromagnetic pulses and record the backscattered signal. The principal scattering mechanism at the oblique incidence angles used in scatterometry is Bragg resonance. Since ocean surface capillary wavelengths and electromagnetic wavelengths are of roughly the same order, scattering from the troughs and crests of the wave field constructively interfere to enhance the measured backscatter power. Bragg scattering is dependent on the observation geometry relative to the scattering wave orientation. An increase in surface roughness due to wind induced capillary waves is accompanied by increased backscattered power.

The normalized radar cross-section, $\sigma°$, is related to the reflected power measurement by the radar equation,

$$P_r = \frac{P_t G^2 \lambda^2 A_{eff}}{(4\pi)^3 R^4} \sigma°$$

where P_r is the received power, P_t is the transmitted power, G is the gain of the antenna in the direction of the scatterer, λ is the wavelength of the transmitted signal, R is the slant range from the antenna to the scatterer, and A_{eff} is the effective area of the scatterer.

As remote sensing instruments, scatterometers do not directly measure vector winds over the ocean. Rather, they infer the wind field from direct measurements of the normalized radar cross-section, $\sigma°$. After illuminating the surface with an radar pulse, a measure of the power in the backscattered signal is used to calculate $\sigma°$, which is related to vector winds by the empirical geophysical model function (GMF).

The GMF expresses $\sigma°$ as a function of wind speed, azimuth angle relative to wind direction (χ), incidence angle (θ), and polarization. As observation geometry and polarization can be controlled by sensor design, a single measurement of $\sigma°$ is effectively mapped to two unknowns, wind speed and direction. In order to achieve a solution, multiple $\sigma°$ measurements must be taken for each given location—termed a wind vector cell (WVC). This is accomplished by varying azimuth angle, incidence angle, and polarization through a variety of sensor design options. The GMF-implied
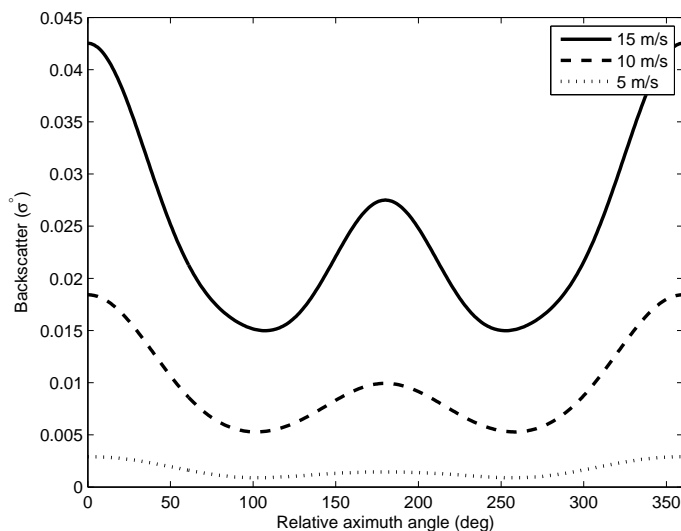
Figure 2.4: Plot of scatterometer $\sigma°$ as a function of wind-direction relative azimuth angle for 5, 10, and 15 m/s and 46° incidence angle

$\sigma°$–azimuth angle relation is plotted in Fig. 2.4 for three different wind speeds. It is sinusoidal in nature and symmetric about the 180° relative azimuth angle. Peaks are positioned in the forward and reverse wind direction azimuths, and troughs in the cross-wind azimuths.

2.2.2 SeaWinds-on-QuikSCAT

Currently, NASA operates one space-borne scatterometer, SeaWinds, aboard the QuikSCAT satellite. It was launched on June 19, 1999 as a quick recovery mission for the successful, but prematurely terminated NASA Scatterometer (NSCAT) mission. Still operating, the QuikSCAT mission has well exceeded its anticipated design lifetime of three years. A second, nearly identical, sensor, SeaWinds-on-ADEOS-II was launched December 14, 2002, but experienced a solar power failure 10 months later. The mission requirements governing the QuikSCAT design are presented in Table 2.2. All requirements were met or exceeded.

QuikSCAT's design is unique from previously launched scatterometers in the

Table 2.2: QuikSCAT Technical Mission Requirements [9]

Quantity	Requirement	Applicable Range
Wind Speed	2 m/s (rms)	3-20 m/s
	10%	20-30 m/s
Wind Direction	20° (rms) selected ambiguity	3-30 m/s
Spatial Resolution	25 km	$\sigma_\circ$ cells
	25 km	wind vector cells
Location Accuracy	25 km (rms)	Absolute
	10 km (rms)	Relative
Coverage	90% of ice free ocean every day	
Mission Duration	36 months	

manner in which is achieves GMF-necessitated azimuth and incidence diversity. Earlier designs used single or multiple fan bean geometries which provide good incidence angle diversity, but have limited azimuth angle diversity. QuikSCAT employs dual scanning pencil bean antennas to achieve excellent azimuth diversity at two separate incidence angles. This observation geometry is diagrammed in Fig. 2.5. The antenna rotates at 18 rpm sweeping out an approximately 1800 km swath with two beams—a horizontally polarized beam at 46° incidence, and a vertically polarized beam at 54° incidence. The resultant helical pattern traced on the surface measures σ° at each 25×25 km WVC at least four times.

From this set of σ° measurements, wind retrieval through the GMF returns up to four possible wind speed and direction combinations called ambiguities. Ambiguity removal algorithms employ 2.5° resolution National Center for Environmental Prediction (NCEP) model winds to "nudge" the selection of of a single wind vector at each WVC and produce the final wind vector field.

2.2.3 Resolution Enhancement

Standard QuikSCAT wind retrieval is obtained on a grid of 25×25 km wind vector cells. The AVE algorithm, developed by Long et al. [10], computes σ° for wind retrieval on a higher resolution grid. The posting of the AVE algorithm grid is 2.5 km.
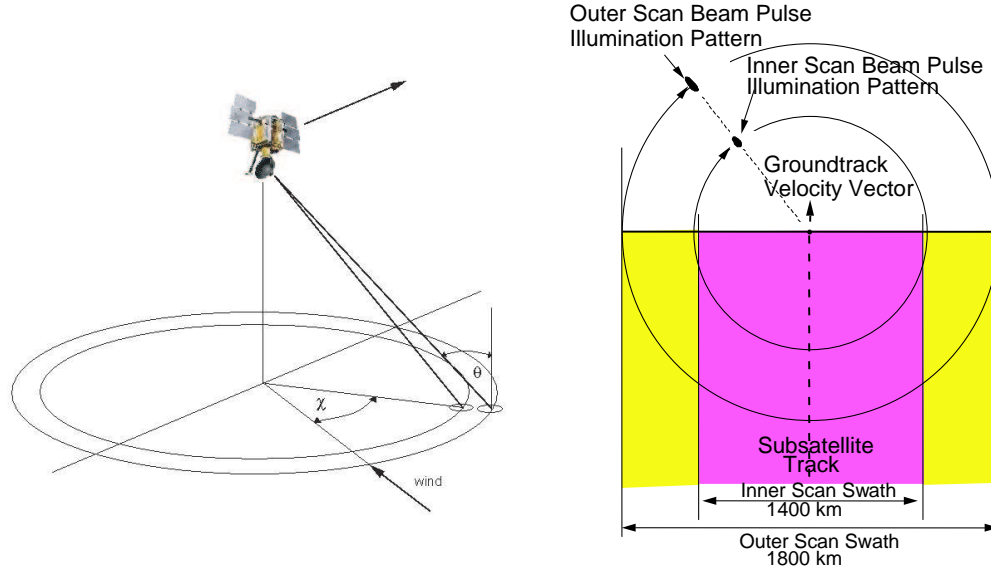
Figure 2.5: QuikSCAT observation geometry.

Enhanced resolution σ° measurements are achieved by range-gating the returned "egg-shaped" scatterometer pulse into smaller "slice-shaped" sub-footprint measurements. The resultant dense spatial oversampling allows creation of an enhanced resolution σ° grid by weighted average and a knowledge of each slice's spatial response function [11].

Four enhanced resolution σ° values are then available at each 2.5 km resolution grid location. Wind retrieval is carried out in a similar manner to standard resolution. Ambiguity removal, however, is complicated because of increased noise in the enhanced resolution σ° field. The resultant wind field has increased resolution but, especially for wind direction, exhibits increased noise.

Chapter 3

Standard and Enhanced Resolution QuikSCAT Observations

Because of its unique ability to infer wind speed *and* direction regardless of cloud cover and solar illumination, QuikSCAT data has proven useful in studying tropical cyclones [1], [2], [4], [3]. QuikSCAT often provides indications of an intensifying storm earlier than other observation systems. Even at its relatively coarse 25 km standard resolution, valuable storm characteristics are evident. This chapter compares a number of storm characteristics and observation conditions viewed at standard and enhanced resolution QuikSCAT data.

Many tropical cyclone characteristics of interest concern the storm's eyewall. Eyewall presence is often visible in the standard resolution QuikSCAT product. Eyewall structure observation, however, frequently requires high resolution. For the purposes of this thesis, we consider storm structure to be entirely defined by the spatial distribution of winds. Eyewall structure, then, is the spatial distribution of the most intense winds in a developed storm. This definition ignores such structural parameters as temperature, pressure, and rain distribution which lie outside the scope of this thesis. In addition to storm structure, an estimate of storm size can be determined from QuikSCAT data. One metric for the size of a tropical cyclone is the diameter of its gale force—about 40 kt (20 m/s)—winds. A typical region of interest encompassing gale force winds for Atlantic hurricanes is about 450 km, though this may be larger in other basins.

A QuikSCAT standard-resolution observation of a hurricane of 450 km covers approximately 19×19 wind vector cells. Typical hurricane eyewalls of developed storms have radii of 10 to 30 km [12]. Consequently, at the standard 25 km QuikSCAT
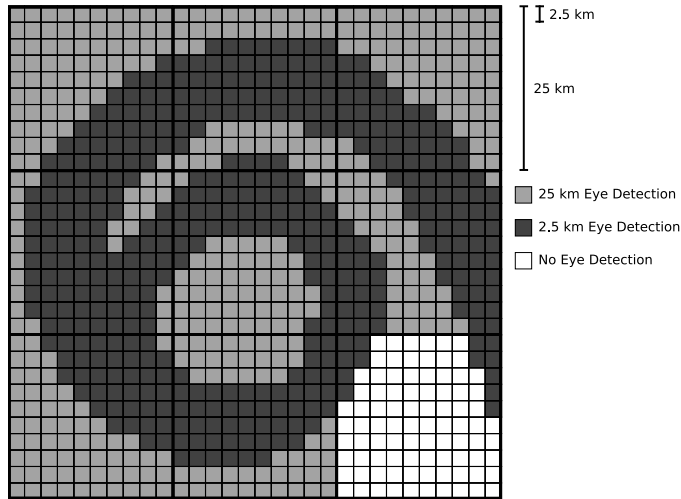
Figure 3.1: Stylized hurricane eye at standard (light grey) and ultra-high (dark grey) resolution. (see text)

resolution, most hurricane eyes lie within an area of 3×3 wind vector cells. At ultra-high QuikSCAT resolution, the same storm is viewed in 180×180 2.5 km cells, and its eye encompasses 24×24 cells. The relative scales of tropical cyclone observation are diagrammed in Fig. 3.1 with a stylized hurricane. In the 25 km wind vector cells (large squares), the presence of eight cells of intense wind speed is shown in the large light-grey shaded squares. Additional structure beyond the presence of intense wind speed is difficult to discern at this scale. In the 2.5 km wind cells (small squares), structure is clearly evident and we are able to estimate the eyewall size to be nine wind cells or 22.5 km in diameter. Although information is available in the standard resolution QuikSCAT data, a significant amount of detail—including important parameters such as structure and size of the inner core, magnitude of winds at the eyewall, and presence of double eye walls—remains undetectable at such scales [13].

QuikSCAT derived wind direction vectors usually indicate a counter-clockwise storm circulation in the northern hemisphere and a clockwise vorticity for southern hemisphere storms. Near the intense eyewall, the reported wind directions are often in error. Three likely reasons for this error are ambiguity selection difficulties, the coarse resolution of the 25 km product, and undetectability of the wind signal due to noise factors such as rain and sea spray and unmodeled characteristics of the sea

surface at high wind speeds. In this chapter, we present tropical cyclone observations at standard (25 km) and ultra-high (2.5 km) resolutions and note the differences in the circulation direction vectors and the wind speed field. We also contrast the visibility of inner core size and structure and double eyewalls through selected storm examples.

3.1   Wind Speed Field

A critical component in tropical cyclone track and intensity forecasting is a good representation of the storm and surrounding wind field. Numerical weather prediction, including tropical cyclone forecasting, is largely an initial value problem. However, initialization data obtained *in situ* are rarely available, especially for the early formation and strengthening stages. This is heightened by the fact that many hurricanes occur far out at sea where direct observation is exceptionally difficult and costly. Satellite data must be relied upon in such cases. Space-borne scatterometry is able to provide highly accurate global wind field data especially for nascent cyclones where the precipitation and wind speeds are relatively low. Even in severe hurricanes, QuikSCAT is able to map the wind speed field within the storm. Recent research has improved the QuikSCAT geophysical model function for severe storm events such as tropical cyclones [14]. Within this thesis, however, we employ the JPL standard QMOD3 geophysical model function [9].

In order to explore tropical cyclone structure, we plot the QuikSCAT derived wind speed field at standard and enhanced resolution. The 25 km wind directions are then overlaid onto the speed field. For the purposes of illustration, we use the standard 25 km product wind directions because of the observed noisiness (Sec. 3.2) in the resolution-enhanced wind directions. A typical observation is shown in Figs. 3.2a (standard resolution) and 3.2b (enhanced resolution). In many cases, as seen in this figure, inferring specifics about the circulation in the storm core from the QuikSCAT direction vectors is difficult. In such cases, the speed field is useful. In the wind speed field at each resolution, general storm structure is evident. The ultra-high resolution field in Fig. 3.2b, however, provides much finer detail. The storm center is more

clearly evident and its circular shape is more apparent. The presence of outer rain bands is detectable, and the structure of the high wind speed eyewall is observable. In Section 3.4 we present additional resolution comparison cases in more detail.
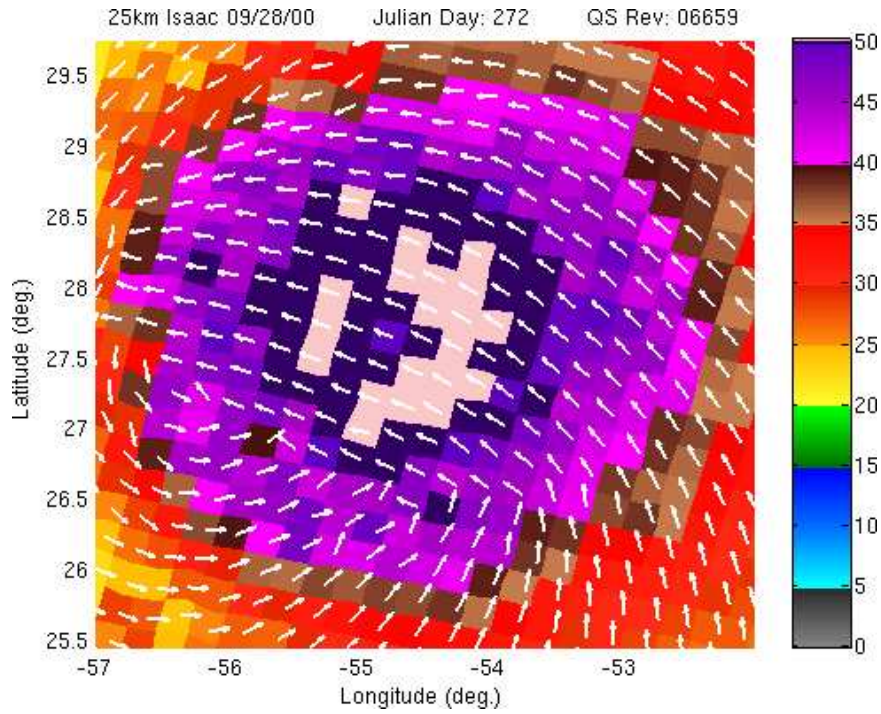
(a)
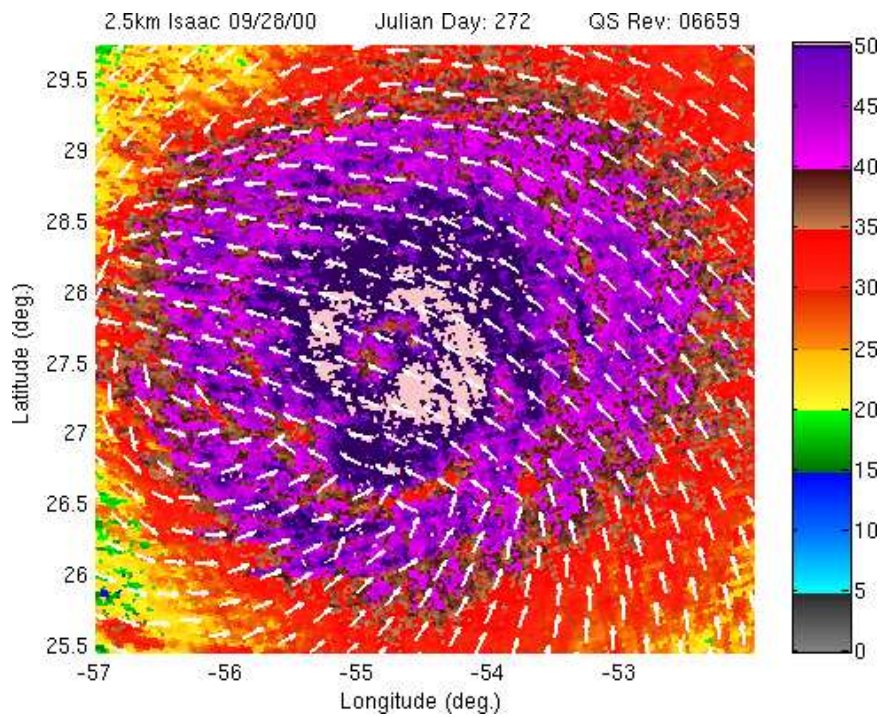
(b)

Figure 3.2: Typical standard (a) and resolution-enhanced (b) QuikSCAT hurricane observation.

3.2 Wind Direction Field

Accurate wind direction information is important in observing and predicting cyclogenesis of new storms and in track and intensity forecasting of developed storms. One sign of an intensifying storm used by Sharp et al. [2] for early detection of cyclones is the vorticity exhibited in the wind direction field. Much of the storm analysis using QuikSCAT is done with images of ambiguity selected wind barbs colored according to the retrieved wind speed as in Fig. 3.3. In this figure we observe the counter-clockwise rotation expected for a northern hemisphere cyclone. Unfortunately, there is an absence of vorticity in the wind direction field at the storm core, due to ambiguity selection error and rain contamination. Instead, the wind direction vectors in this region exhibit a nearly uniform west-northwest direction. This is a representative instantiation of the cross-track pinning of the wind direction field from intense precipitation within the footprint of the sensor, coupled with ambiguity selection errors.

Wind direction vectors from resolution enhanced retrieval are inherently noisier than those retrieved at standard resolution [15]. This is evident from the example in Fig. 3.4. In this figure we have overlaid standard (Fig. 3.4a) and ultra-high (Fig. 3.4b) resolution wind direction vectors onto the resolution-enhanced wind speed field. In order to maintain visibility of the underlying wind speed field, this figure shows every 15th resolution enhanced wind direction. The ambiguity selection algorithm used in this processing selects the ultra-high resolution ambiguity closest to the selected standard resolution ambiguity. For this reason, circulation centers obtained only from ultra-high resolution wind directions are not expected to differ significantly from standard resolution circulation centers, with the exception of additional noise. In future figures, we therefore overlay standard resolution wind directions, as opposed to the resolution enhanced wind directions, onto the ultra-high resolution wind speed field for storm observations throughout this study.
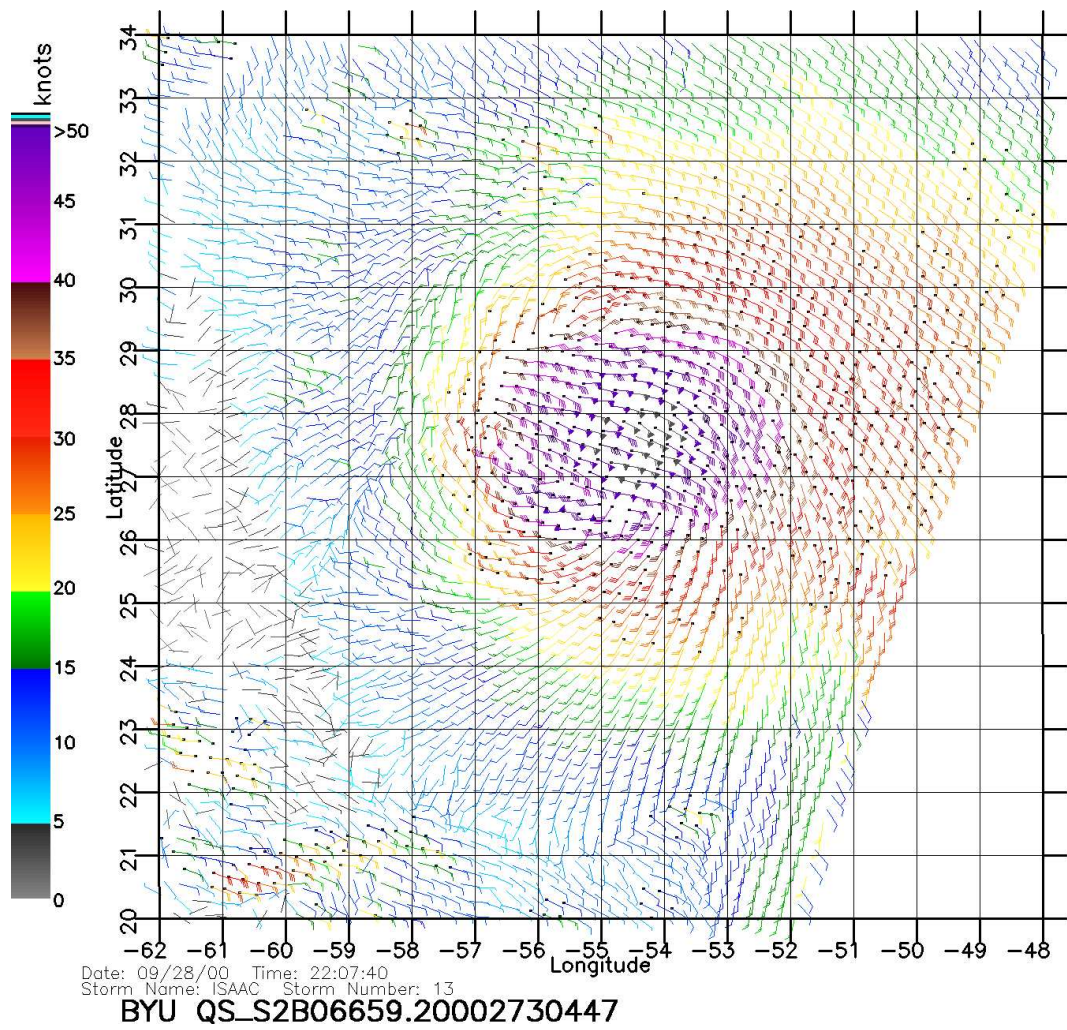
Figure 3.3: Ambiguity selected wind direction barbs colored according to wind speed.
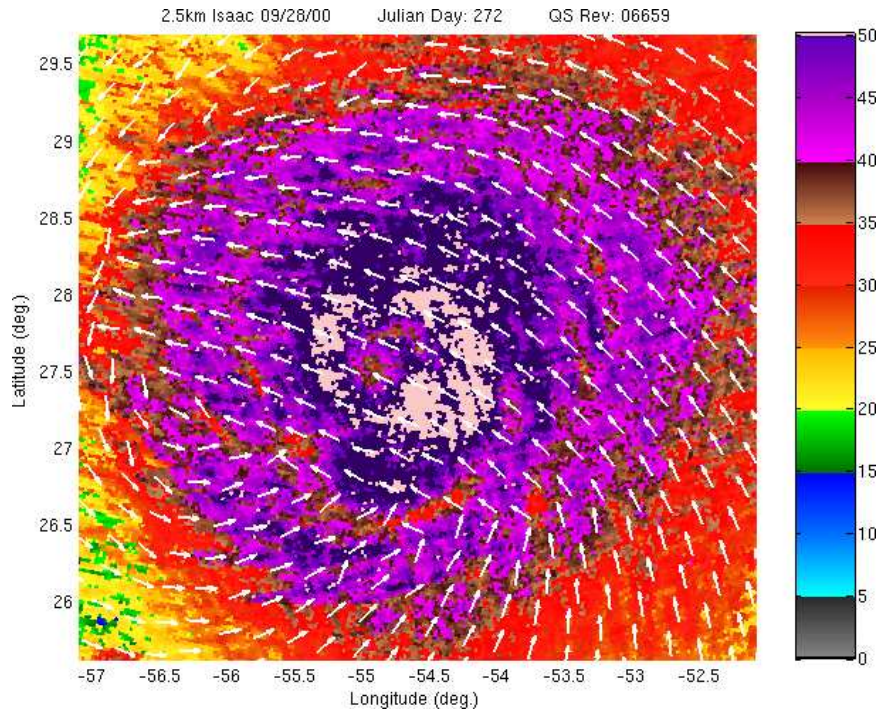
(a)
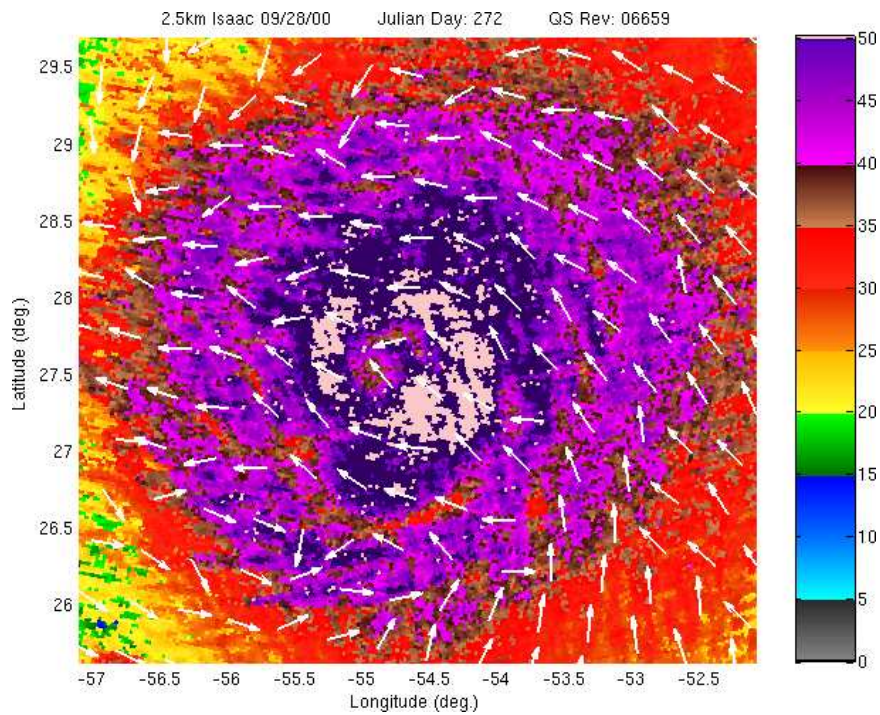
(b)

Figure 3.4: Standard (a) and ultra-high (b) resolution wind direction vectors overlaid onto ultra-high resolution wind speed field

3.3 Complications of Wind Retrieval in Tropical Cyclones

Part of the difficulty in remotely sensing near-surface wind speed in tropical cyclones lies in the un-modeled effects of intense wind speed over the ocean surface. At high wind speeds, the ocean surface behaves differently as the capillary waves used to infer winds are masked by sea spray and foam. Even with detailed models which account for this change of behavior, validation is difficult due to hostile and isolated *in situ* environments. Further complicating the task—and perhaps most significant—are the effects of heavy rain on the backscattered radar signal. A simple phenomenological backscatter model,

$$\sigma_m = (\sigma_w + \sigma_{sr})\alpha_r + \sigma_r$$

illustrates the effects of rain on the scatterometer measurements. The measured backscatter, σ_m (which is ideally equal to the wind-induced backscatter, σ_w), is altered by rain impacting the ocean surface, σ_{sr}. As rain strikes the water, it induces feature changes such as ripples, stalks, and crowns which affect the surface backscatter. Raindrops striking the ocean surface are also thought to dampen the wind-induced capillary waves. While airborne, raindrops cause two-way attenuation, α_r, and volume backscattering, σ_r, of the Ku-band radar signal.

Draper and Long used this model to evaluate the effects of rain on QuikSCAT [16] and then to devise a method to simultaneously retrieve wind and rain with the sensor [17]. Within this development, they classified wind and rain retrieval conditions into three regimes based on the relative retrievability of each parameter. Observations may be rain-dominated, wind-dominated, or of the equal order. Rain-dominated observations occur when rain factors ($\alpha_r\sigma_{sr}$ and σ_r) are very large with respect to the rain-attenuated, wind-induced backscatter ($\alpha_r\sigma_w$). Such conditions often occur in the cores of developed tropical cyclones. A tell-tale sign—but not a failsafe indicator—of rain-dominated observations within a QuikSCAT wind field is pinning of the retrieved wind directions in a cross-track direction. Additionally, cross-track pinning degrades the reliability of ambiguity removal algorithms. In such senarios, it is difficult to ascertain what is actually represented in the QuikSCAT

retrieved wind field. It is likely that these fields largely portray parameters of the rain rate with little actual contribution from the wind. Nonetheless, tropical cyclone structure is still inferrable in this 'wind field' with the understanding that what is reported as wind speed and direction may actually represent other quantities.

Outside the cores of tropical cyclones, QuikSCAT winds are very accurate [18]. QuikSCAT design specifications require that the scatterometer measure winds with no more than the greater of 2 m/s (rms) or 10% error for wind speeds between 3 and 30 m/s (see Table 2.2). The design specifications place no constraints on the required accuracy of data collected over extreme wind speed regions such as the cores of tropical cyclones. These typically fall outside the applicable range of the wind speed accuracy requirement[9]. Though QuikSCAT was not designed for wind retrieval in hurricanes, within limitations it is reasonably accurate.

3.4   Selected Storm Examples

In this section we present several cases of example storm observations depicting various storm and observation conditions. The conditions of interest are inner core size and structure, presence of double eyewalls, observations near land, and cases of ambiguous storm centers. These examples illustrate several areas of difference in standard and resolution enhanced QuikSCAT observation of tropical cyclones.

3.4.1   Inner Core Size and Structure

The damage potential of tropical cyclones is closely related to the size and structure of the inner core. The evolution of inner core structure is also important in tropical cyclone intensity forecasting. To explore the retrievability of this structure, we present three hurricanes of varied intensity at standard and ultra-high resolution and compare visible features. The storms considered are Lisa (2004), Frances (2004), and Katrina (2005). These storms represent various scales of size, developmental stage, and intensity.

Hurricane Lisa was a relatively-long lived tropical cyclone. It formed as a tropical depression off the coast of Africa on September 19, 2004 and dissipated off the
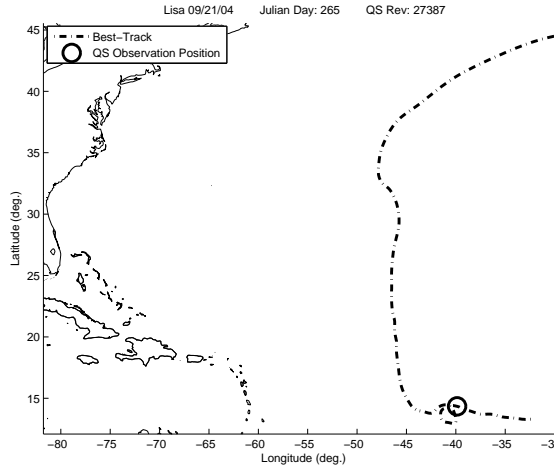
Figure 3.5: National Hurricane Center best-track of Hurricane Lisa (2004).

coast of Newfoundland on October 3, 2004. Hurricanes forming off the coast of Africa are termed Cape Verde-type hurricanes. They are often very intense and long-lived because of the expanse of open ocean over which they can maintain intensity. Lisa, however, stayed relatively weak due to unfavorable intensification conditions caused primarily by two competing tropical systems—Hurricane Karl to the west-north-west and a large, convectively active system to the southeast. Maximum intensity winds, at 65 kt, were sufficient to warrant a Category 1 Hurricane classification for only 12 hours out of about two weeks as a tropical cyclone. Because it remained relatively weak and far from land (see Fig. 3.5), there were no reports of damage or casualties associated with Hurricane Lisa [19].

Due to its longevity, Hurricane Lisa was viewed several times by QuikSCAT. In total, 21 QuikSCAT revs view part or all of Hurricane Lisa. The location of one of these observations is shown by the circle in the NHC best track in Fig. 3.5. This observation, taken from QuikSCAT rev 27387 on September 21, 2004, views Lisa just after strengthening to a tropical storm. Figure 3.6 shows the QuikSCAT wind field from this observation for a region around Lisa. The standard resolution wind speed field and the resolution enhanced wind speed field are plotted in Figs. 3.6a and 3.6b respectively; both are shown beneath the standard resolution wind direction arrows.

At standard QuikSCAT resolution (Fig. 3.6a), Hurricane Lisa on September 21, 2004 appears as a cyclonic storm with a high wind speed core. Circulation is clear in the outer regions of the storm. In the highest wind speed region, though, there are ambiguity and rain contamination errors. These errors obscure the structure of the developing core. The resultant obscurity and the relatively small storm core size lead to difficulty in identifying the storm center and in understanding the characteristics of the eyewall.

Comparing the standard resolution wind speed field in Fig. 3.6a to the resolution enhanced version in Fig. 3.6b reveals additional details in the latter. The two wind speed fields at the standard and enhanced resolutions are similar. Both indicate the same order of wind speed—about 45 knots at the core and decreasing radially. General storm structure in each is also comparable. In the 2.5 km image, though, a drop in wind speed of approximately 15 to 20 knots across the core is visible. This feature delineates the storm's eyewall. Figure 3.6b enables less uncertainty in locating the circulation center compared to the standard resolution wind speed and direction fields. In addition to the presence of an eyewall, the ultra-high resolution image also depicts its asymmetry.

The northern part of the storm core contains many more cells of wind speed above 40 knots than does the southern part. The greater number of high wind speed cells in the northern part of the core may be due to the gross motion of the storm and resultant asymmetry across the direction of forward movement (see Sec. 2.1.2). For tropical cyclones in the Northern Hemisphere, higher wind speed in the northern part of the storm relative to the southern part are seen in westward moving storms. From Figure 3.5, the storm is moving roughly westward at the time of this QuikSCAT observation. Existence and structure of Hurricane Lisa's developing eyewall, including its asymmetry, is more easily perceived in the resolution enhanced wind speed field.

At Category 4, the peak intensity of Hurricane Frances (2004) was greater than that of Lisa. Upon its landfall in the Bahamas as a Category 3 hurricane and then in Florida as a Category 2 on the Saffir-Simpson scale, Frances was directly responsible for $4.43 billion in damage and 7 deaths. An additional 42 deaths are
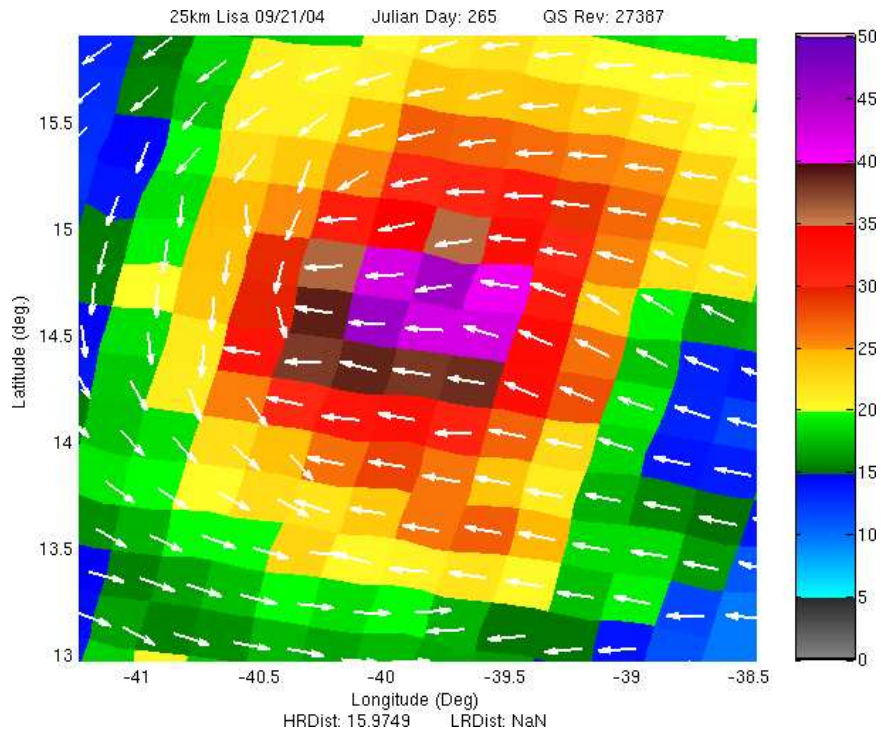
(a)
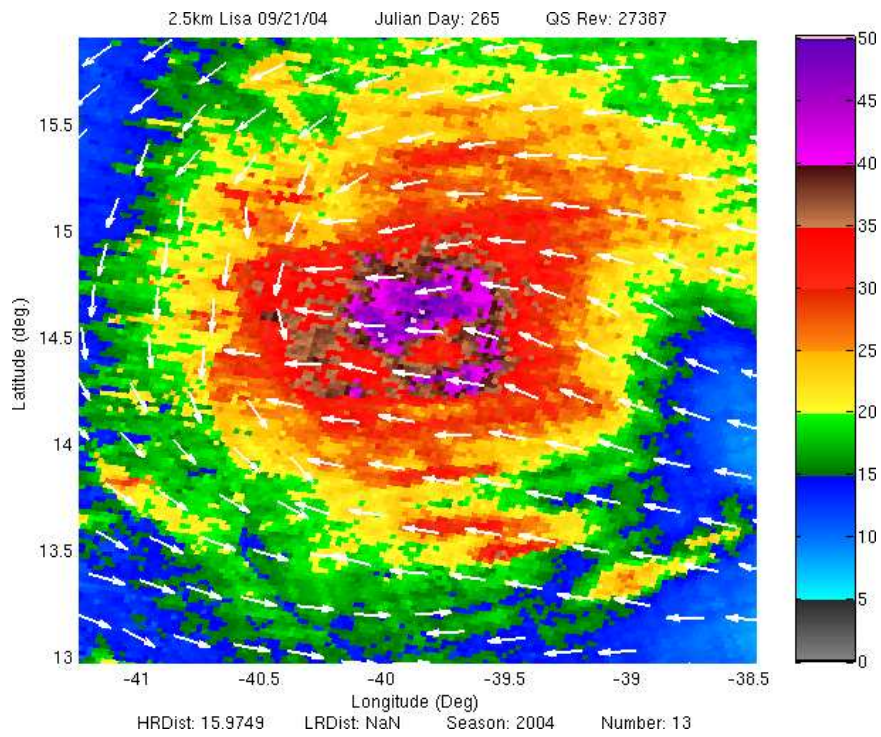
(b)

Figure 3.6: Structure of Hurricane Lisa in 2004. (a) standard resolution (b) ultra-high resolution.
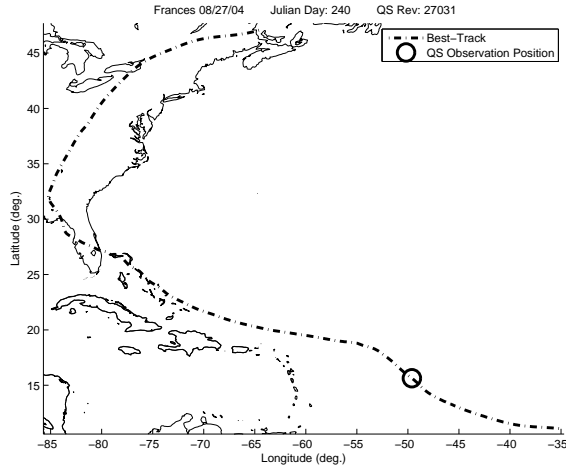
Figure 3.7: NHC best track of Frances (2004). The QuikSCAT observation in Fig. 3.8 occurred at the location indicated by the circle.

indirectly attributed to Frances. As depicted in the NHC best track in Fig. 3.7, Hurricane Frances formed off the shore of Africa as a Cape Verde type hurricane and moved northwest toward the south-eastern coast of Florida. As with Hurricane Lisa, Frances was viewed a number of times within the QuikSCAT swath—18 QuikSCAT revs in total. One of these observations occurred on August 27, 2004 at UTC 21:46 in rev 27031. This observation is depicted in standard and ultra-high resolution in Fig. 3.8 and its location is indicated by the circle along the best track in Fig. 3.7.

On August 27, 2004 at the time of QuikSCAT observation, Frances had reached hurricane status and was undergoing further intensification. Its maximum sustained wind speed at the time is estimated by the NHC to be 100 knots. Figures 3.8a and 3.8b present the wind speed fields of this well developed storm at standard and enhanced resolution respectively. The standard resolution wind direction field is plotted on top of the speed field in each case.

The wind direction field, in this example, exhibits reasonable vorticity throughout the storm—including within the core. Ambiguity and precipitation errors are not as obvious as they were in the observation of Hurricane Lisa. Consequently, some storm core structure is evident within this wind direction field.

Wind speeds in three QuikSCAT wind vector cells are in excess of 50 kt. The

magnitude of these three cells indicates the presence of a well developed core. Related to conservation of angular momentum, intense, well-developed tropical cyclone cores are often small in size. The well-developed core of Hurricane Frances in this observation exhibits this small size. In the 25 km image, the highest wind speed region encompasses only 3×3 cells, approximately. Further details about its structure are difficult to perceive.

At ultra-high resolution, much of the storm's core structure is visible. Several cells with wind speed greater than 50 kt are organized in a nearly complete circular arrangement. This set of cells outlines a majority of the hurricane eyewall. Within this arrangement, a region of lower wind speed clearly represents the eye. We note that this region is somewhat offset from the perceived center of vorticity in the L2B direction arrows.

As with Hurricane Lisa, asymmetry is present in the observation of Frances' core. Higher wind speeds are retrieved for the northern and eastern portions of the storm's core. A line, which we call the axis of asymmetry, running approximately from southeast to northwest divides the higher wind speed portions of the core from the lower wind speed portions. In Fig. 3.7, the storm is shown to be moving roughly northwest. That the axis of asymmetry matches with the overall storm movement is, again, perhaps indicative of forward-movement induced asymmetry. This phenomenon is imperceptible at standard QuikSCAT resolution.

Hurricane Katrina (2005) was the costliest storm to ever hit the United States with an estimated \$75 billion in damage [20]. It was also one of the five deadliest with approximately 1300 directly or indirectly attributed deaths. It first impacted the southern tip of Florida as a Category 1 hurricane on the Saffir-Simpson scale. Then, after moving into the Gulf of Mexico it strengthened into a large Category 5 hurricane. Figure 3.10 shows the wind speed (knots) and direction of Katrina while it was an exceptionally large Category 5 hurricane off the Gulf coast. This observation is taken from QuikSCAT rev 32251 on August 28, 2005 (JD 240) at UTC 23:49. In this figure, the storm is just beginning a rapid weakening. Within a few hours Katrina had reached landfall and weakened to a Category 3 hurricane. Most of the storm's

(a)
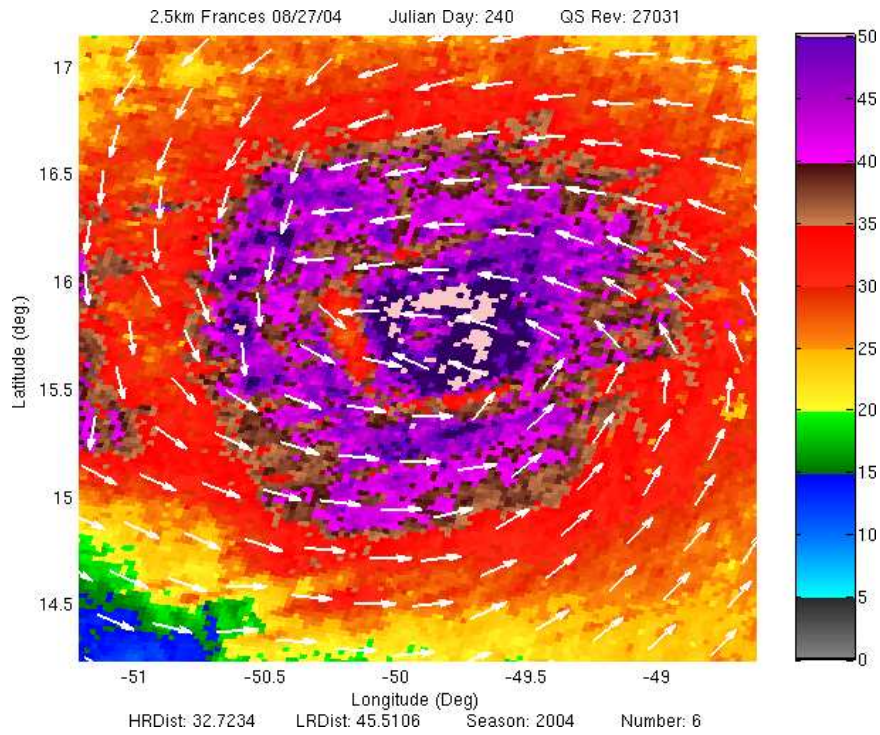
(b)

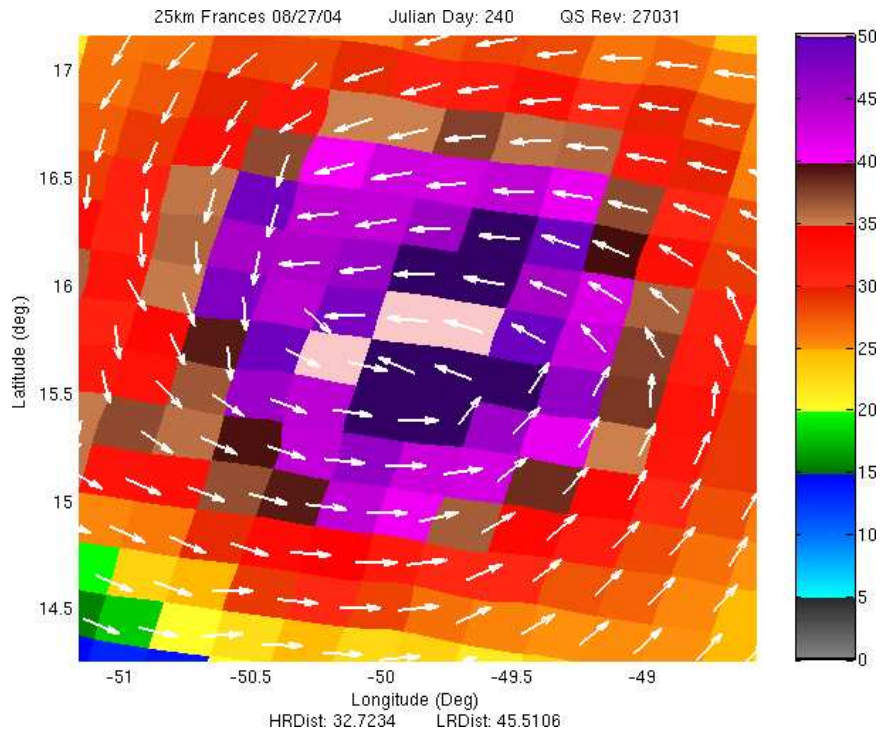Figure 3.8: Eyewall structure of Hurricane Frances in 2004. (a) standard resolution (b) ultra-high resolution
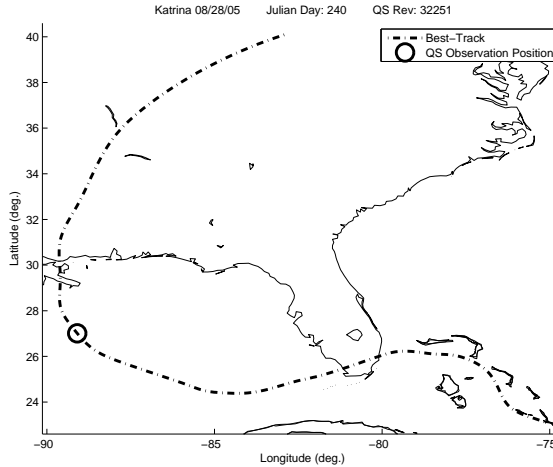
Figure 3.9: NHC best-track of Katrina (2005). The QuikSCAT observation in Fig. 3.10 occurred at the location indicated by the circle.

damage came at landfall on the Gulf coast in Louisiana and Mississippi just after it weakened to Category 3. The National Hurricane Center's 'best track' is shown in Fig. 3.9. The location of the QuikSCAT observation in Fig. 3.10 is indicated by the circle along the track in th Gulf of Mexico.

In the standard resolution image (Fig. 3.10a) significant detail regarding the wind structure is visible. This is aided by Katrina's large size. A large number of wind speeds in excess of 50 kt are detected in the core. The counter-clockwise vorticity is evident at the fringes of the storm. Within its core, precipitation-caused direction errors erode the clarity of the circulation center. The storm center can be roughly inferred from the center of the intense wind speed field, however.

Comparing Fig. 3.10a with the resolution-enhanced version in Fig. 3.10b, additional details are evident. Outer convection bands, seen as semi-circular regions of intense wind speed outside of the inner core, are differentiable from the eyewall. The scope and clearly defined nature of the eyewall are evident. There is greater wind speed contrast at the eyewall. Another significant feature in the ultra-high resolution image is the presence of concentric eyewalls. A smaller, weaker eyewall is observed within the intense outer eyewall. Additional observations of this phenomenon are

considered in Sec. 3.4.2. In this figure, the inner eyewall is seen deteriorating. Hurricane Katrina's rapid weakening before landfall is primarily attributed to this change in internal structure [20].
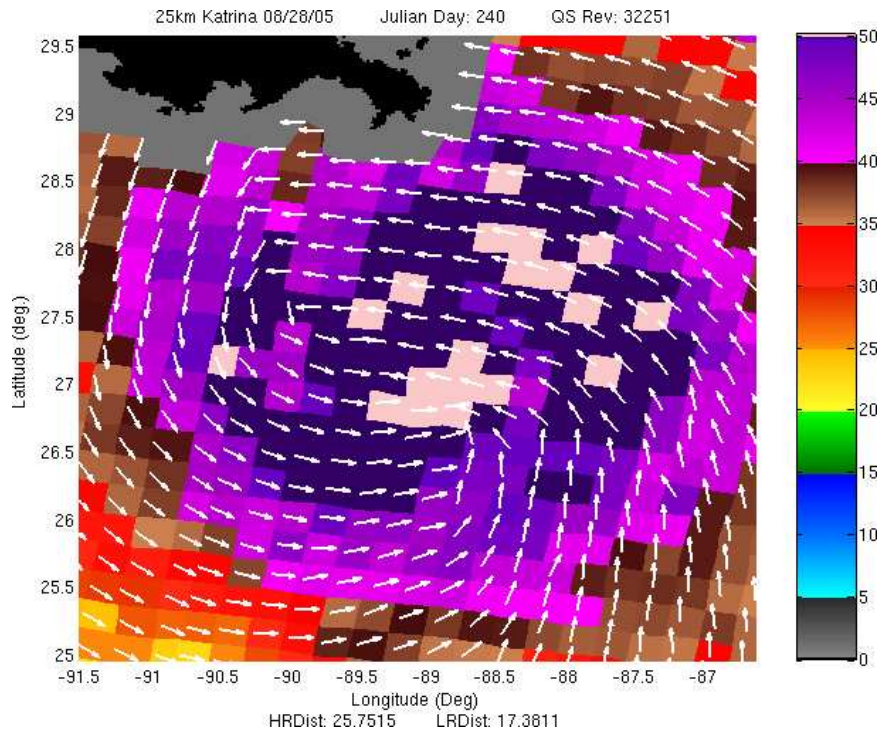
(a)
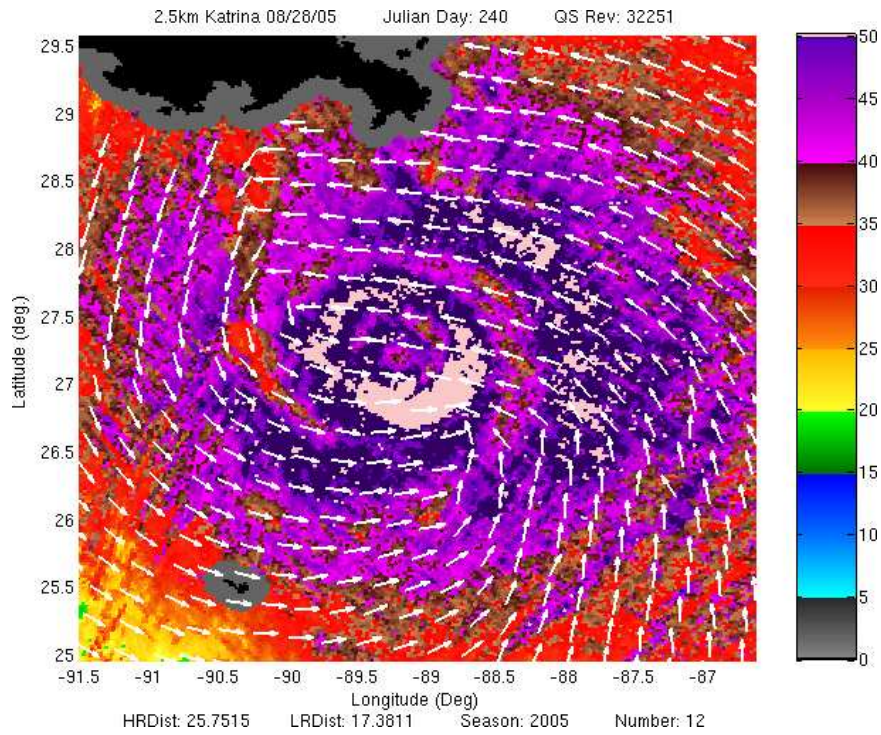
(b)

Figure 3.10: Storm structure of Hurricane Katrina in 2005. (a) standard resolution
(b) ultra-high resolution

3.4.2 Concentric Eyewalls

Intense tropical cyclones frequently exhibit concentric eyewalls [21]. As wind intensity reaches about 100 knots (50 m/s), the storm's eyewall radius often contracts to a very small size—around 25 km. Outside of this small eyewall, some of the outer rain bands may organize into a convective ring that slowly shrinks in radius. This newly formed ring is termed a secondary, or concentric, eyewall. As it contracts, it monopolizes the available moisture and momentum at the expense of the original (inner) eyewall. During this phase, the storm may weaken, or halt intensification. Eventually, the inner eyewall dissipates completing the eyewall replacement cycle. Knowledge of the eyewall replacement cycle is important in understanding the inner core dynamics and projecting short-term intensity changes, and for modeling simulations and upgrading landfall warnings [22]. In this section, we present a sequence of wind field images, at standard and enhanced QuikSCAT resolution, of the evolution of concentric eyewalls in Hurricane Isabel (2003). We also display an observation of Hurricane Katrina (2005) which shows the storm beginning the final stage of eyewall replacement.

In 2003, a wind speed measurement of Hurricane Isabel reported 203 kt, the strongest ever observed in an Atlantic Hurricane [23]. Hurricane Isabel formed as a Cape Verde storm on 6 September 2003, and was long-lived, moving across western Pennsylvania on 19 September 2003. It reached Category 5 status on the Saffir-Simpson Scale and was directly responsible for 16 deaths and $1.7 billion in damage. It made landfall in North Carolina as a Category 2 hurricane and primarily affected parts of North Carolina, Virginia, and New England.

Before its landfall, Isabel formed a secondary eyewall [23]. This formation was observed by a sequence of QuikSCAT and SeaWinds passes from 16 to 18 September 2003. Three of these observations are shown in Figs. 3.12, 3.13, and 3.14. The NHC best track for Isabel is shown in Fig. 3.11 with the locations of the three QuikSCAT observations indicated by the circles along the track.

On 16 September 2003 at 22:26 UTC, QuikSCAT rev 22098 observed Hurricane Isabel. The wind speed and direction fields for this observation are depicted
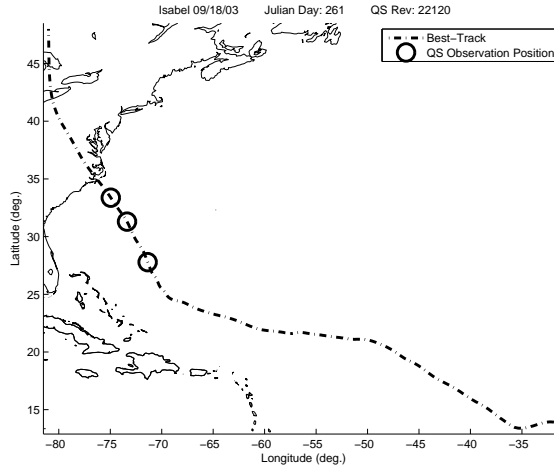
Figure 3.11: National Hurricane Center best-track of Hurricane Isabel.

in Fig. 3.12. At the time, a secondary eyewall within the storm was beginning to form. At standard resolution, it is difficult to distinguish the inner and outer rings. A longitudinally oblong region of high retrieved wind speed is apparent and a lower wind speed eye visible within its circumscription. The presence of a second eyewall, though, is not obvious at 25 km resolution.

Using 2.5 km enhanced resolution images, the forming ring is more apparent. What appears as a single elliptical eyewall at standard resolution is interpreted at enhanced resolution as a more circular eyewall in the western part of the figure with a comma-shaped high wind speed region to the east. The inner eyewall is not completely closed, but is sufficiently outlined to infer the circular nature. The comma-shaped depiction of the outer rain band is beginning to wrap around the rest of the storm's core, eventually to form a secondary eyewall.

Another observation about 24 hours after Fig. 3.12 views the secondary eyewall as more enveloping of the inner eyewall. It is shown in Fig. 3.13 and represents QuikSCAT rev 22113 from 23:39 UTC on 17 September 2003. The standard resolution observation in Fig. 3.13a portrays a well developed storm with a high wind speed eyewall and a lower wind speed eye. Details of the concentric eyewall formation, however, are difficult to recognize. A single large eye is the most readily apparent

37
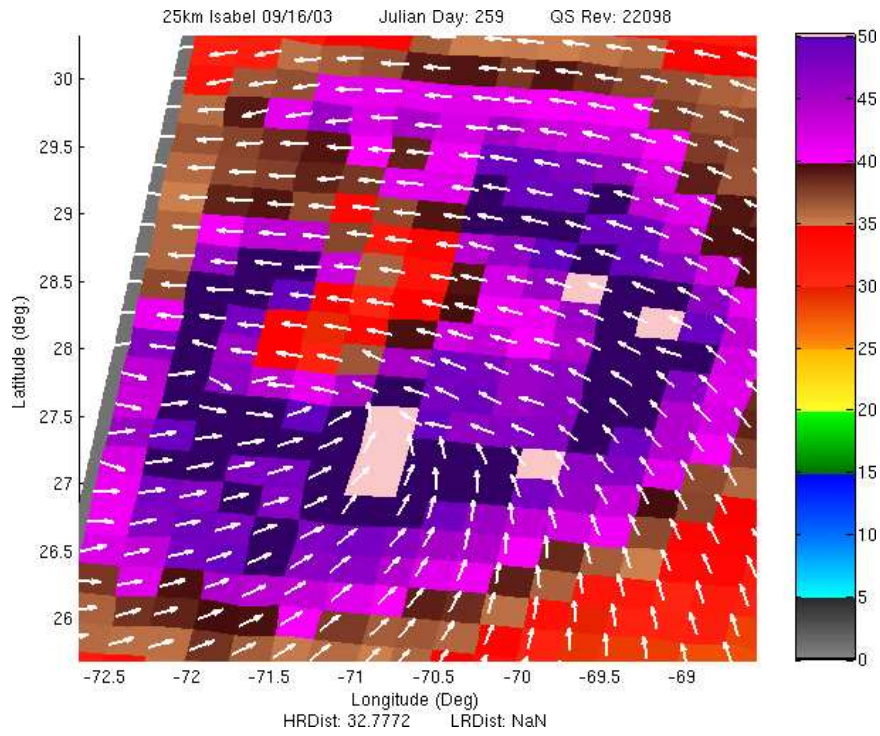
(a)
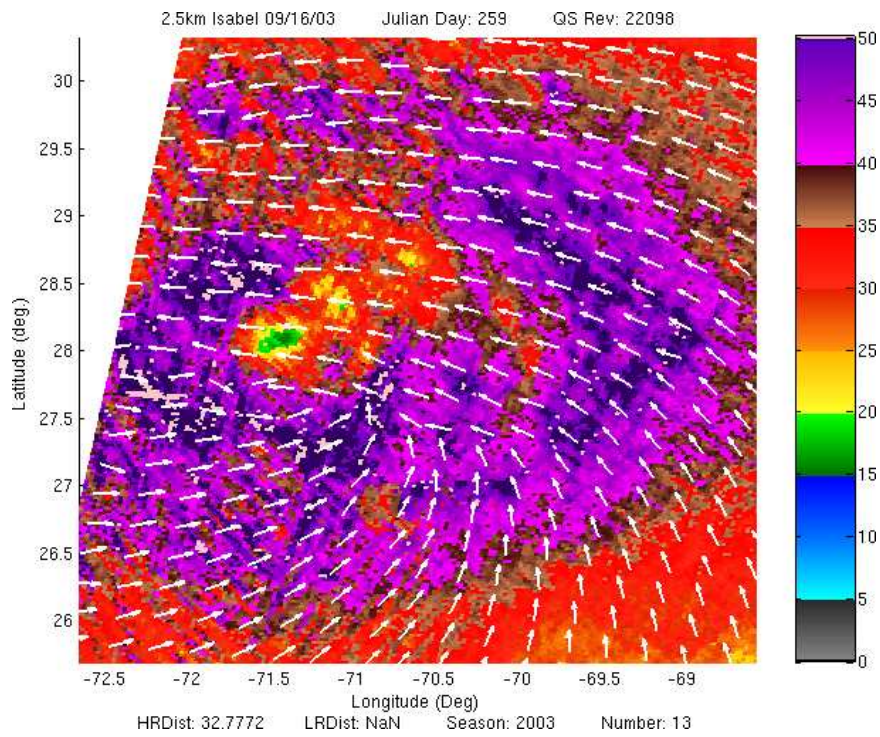
(b)

Figure 3.12: Outer eye forming in Hurricane Isabel in 2003. (a) standard resolution (b) ultra-high resolution

38

interpretation of the standard resolution wind speed field.

To observe the outer rain bands organizing into a secondary eyewall, we examine the resolution-enhanced QuikSCAT wind field in Fig. 3.13b. We see the eye clearly depicted at the center of the image. Surrounding the eye, the inner eyewall is much more visible at enhanced resolution. The inner eyewall contrasts with the lower wind speed trough just outward from it. As the secondary eyewall constricts, this trough will shrink to become the new eye at the completion of the eyewall replacement cycle. That this trough encircles a large portion of the eyewall is indicative of concentric eyewalls. The secondary eyewall is located just outside of the trough and is the feature seen as the primary eyewall in the standard resolution figure (Fig. 3.13a). Following this stage, the inner eyewall continues to weaken and is enveloped by the constricting outer eyewall.

QuikSCAT rev 22120 on 18 September 2003 offers a view of Isabel's fully developed secondary eyewall. The outer eyewall has constricted significantly and is beginning to erode the primary eyewall. This observation is depicted in Fig. 3.14 at standard (a) and enhanced (b) resolutions. Note that the wind direction vectors for this observation appear reasonable and there are no clear signs of ambiguity selection errors or rain contamination. The L2B wind directions clearly depict the position of the storm vortex center. They do not, however, indicate evidence for concentric eyewalls. To examine the eyewall structure we once again refer to the wind speed field. Similar to Figs. 3.12 and 3.13, the 2.5 km enhanced resolution wind speed field provides a clearer picture of the concentric eyewall structure. Only a single large eyewall is visible at 25 km resolution. At ultra-high resolution, the eroding inner eyewall is clearly visible. Surrounding it is an exceptionally large secondary eyewall. To further illustrate the final stage of the eyewall replacement cycle as observed by QuikSCAT, we display an observation of beginning eyewall replacement in Katrina (2005).

On 28 August 2005 at 11:27 UTC, QuikSCAT rev 32244 observed Hurricane Katrina at near-peak intensity. By 18:00 UTC on 28 August, Katrina would be the one of the most intense Category 5 Atlantic hurricanes on record with wind speeds
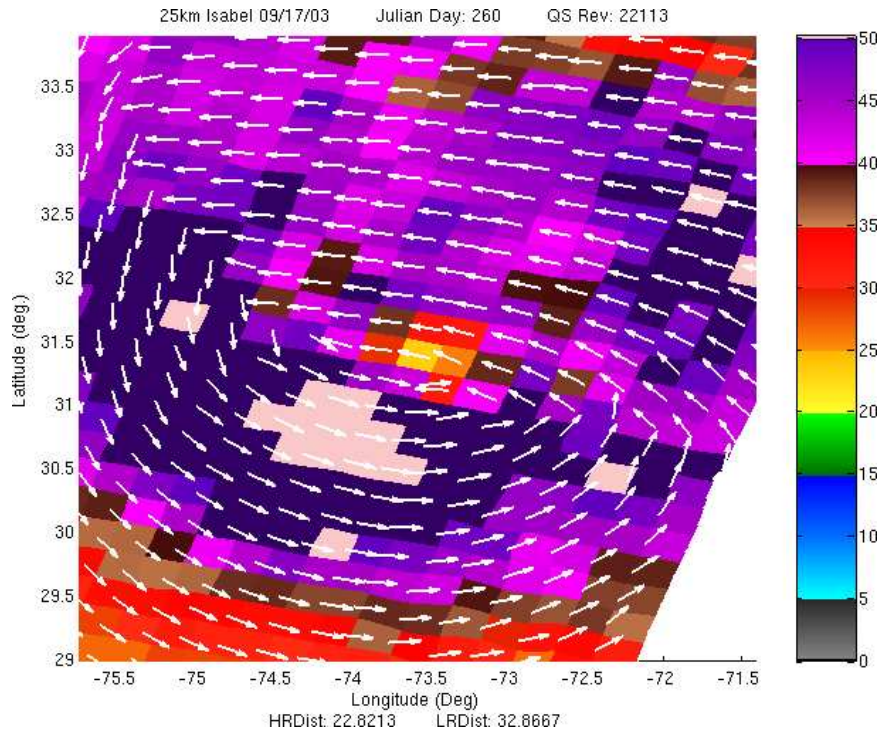
(a)
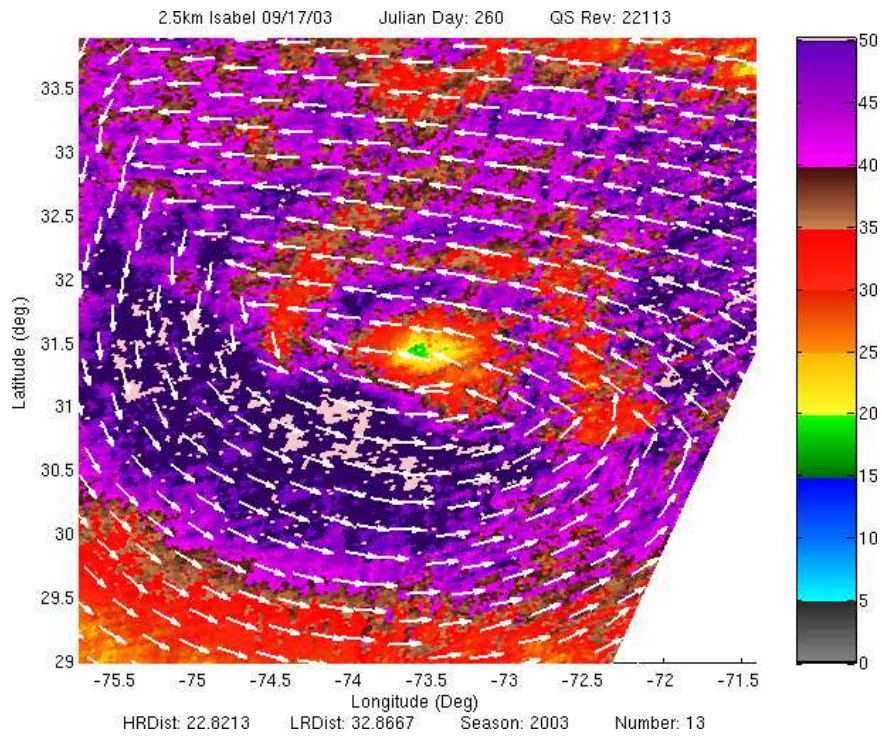
(b)

Figure 3.13: Concentric eyes in Hurricane Isabel in 2003. (a) standard resolution (b) ultra-high resolution
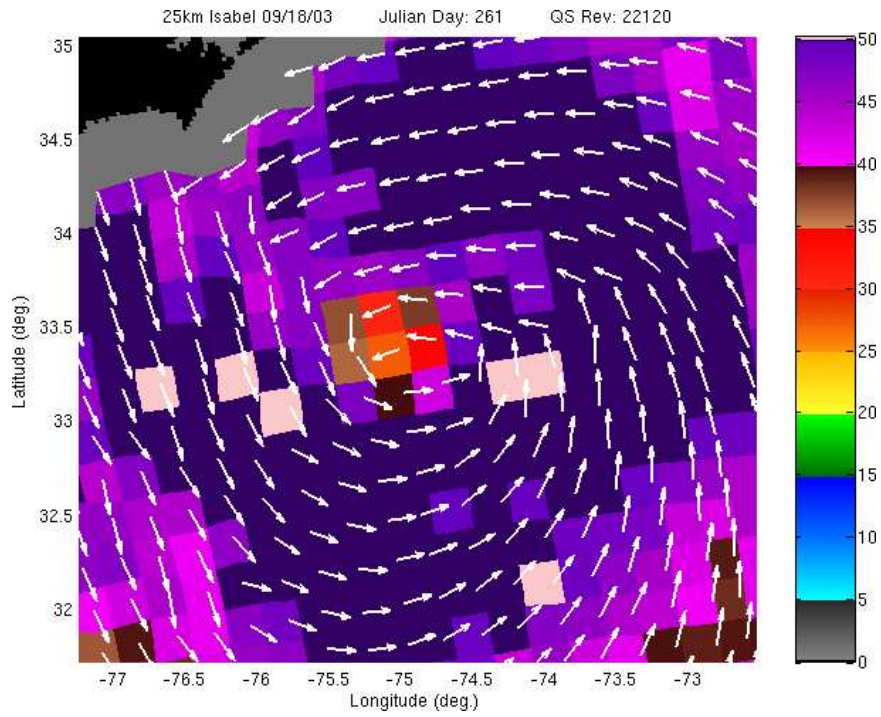
(a)
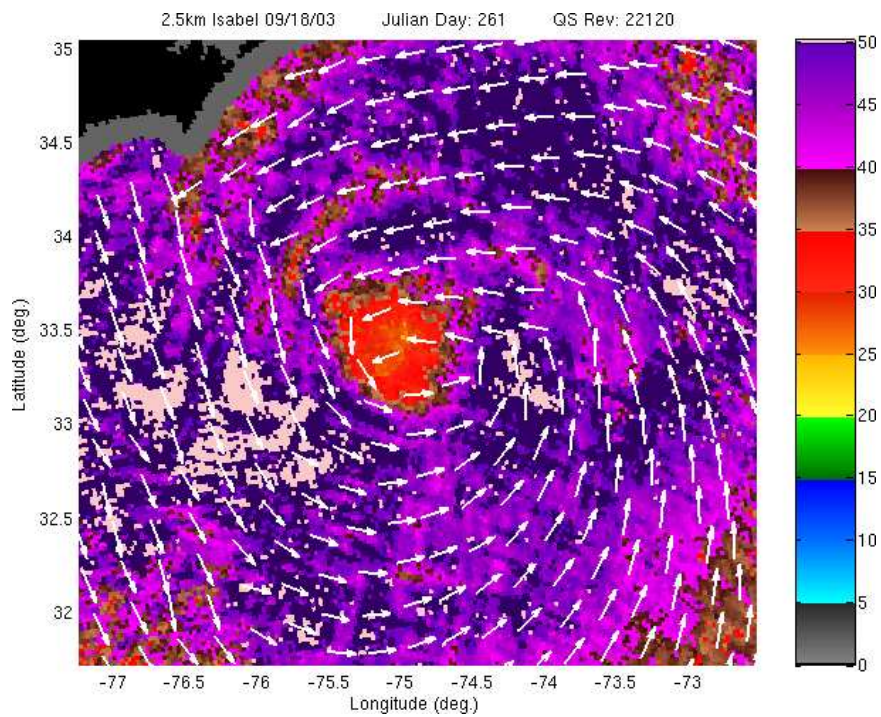
(b)

Figure 3.14: QuikSCAT observation of large secondary eyewall in Isabel in 2003. (a) standard resolution (b) ultra-high resolution

of 150 kt. Earlier, on 27 August, a secondary eyewall formed within Katrina. Over the course of the following day, this outer eyewall contracted until late on the 28th the inner eyewall had completely eroded. In the standard resolution QuikSCAT observation (Fig. 3.15a), the dual-eyewall presence is imperceptible. Only a single, intense eyewall is visible. Observing with ultra-high resolution, however, the pinhole inner eyewall is apparent in the northern and southern portions of the core. This inner eyewall is in the midst of a replacement cycle due to the contraction of the secondary eyewall. The structural changes resultant from this eyewall replacement cycle caused a rapid weakening in Hurricane Katrina. By landfall on 29 August, the storm had weakened to a Category 3 with estimated intensity of 110 kt. Even with this substantial weakening, Katrina still caused incredible damage to much of the north-central Gulf coast. In Section 3.4.3 we explore the differences in standard and enhanced resolution QuikSCAT wind speed fields for observations made at landfall of storms along the coast.
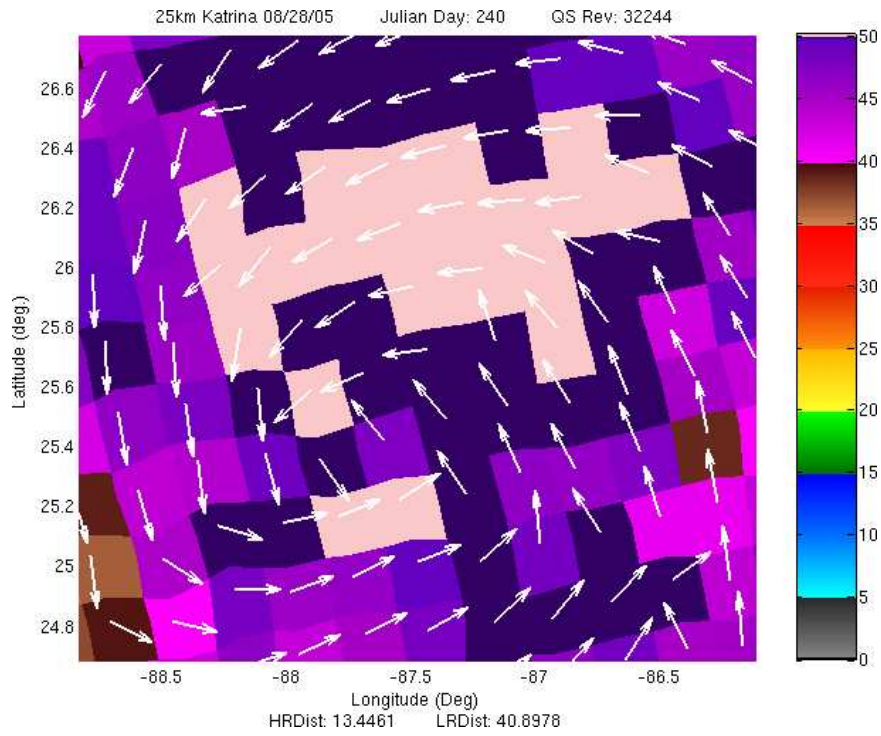
(a)
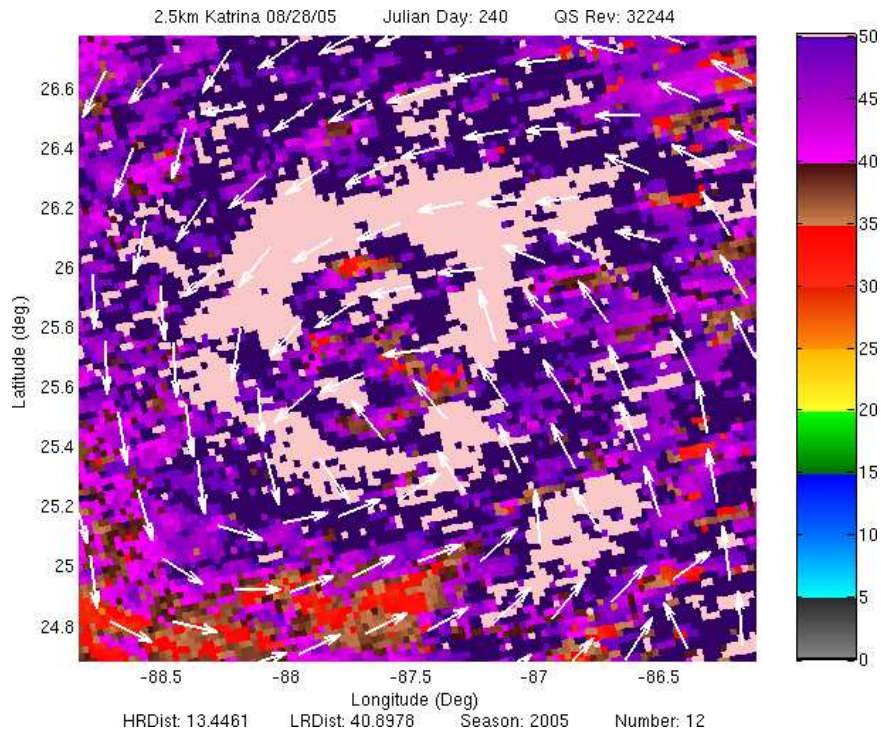
(b)

Figure 3.15: Eyewall replacement in Hurricane Katrina in 2003. (a) standard resolution (b) ultra-high resolution

3.4.3   Near Land

Near the coast, backscatter measurements are contaminated by land within the sensor footprint. Since the geophysical model function used by QuikSCAT to infer the near surface wind field is valid only over open ocean, near-land observations are problematic. Additionally, the behavior of the ocean surface changes due to the boundary effects of the coast. Because of these factors, QuikSCAT standard processing includes a near-to-land exclusion mask for data within about 1 WVC (30 km) of land [9]. Ultra-high resolution QuikSCAT winds are retrieved right up to the coastline, though some of these estimates are contaminated by land. Within this thesis, we use images with a post-wind-retrieval mask applied to data within 15 km of land. Most land contaminated ultra-high resolution wind estimates are masked at this range. The smaller mask affords a view of somewhat more of the storm at landfall. This section focuses on the differences in standard and enhanced resolution wind retrieval for tropical cyclone observations near landfall. We present views of two storms of differing intensity—Ophelia (2005), and Wilma (2005).

Hurricane Ophelia, a relatively weak tropical cyclone, was viewed at near-landfall in North Carolina. Ophelia became a tropical depression on 6 September 2005 near the Bahamas and fluctuated in intensity between tropical storm and Category 1 hurricane several times. It reached its peak intensity of 75 kt twice. The first time occurred in open ocean on 11 September, and the second time on 15 September as it passed near and generally parallel to the North Carolina coast [24]. During this time, the northern and western portions of the eyewall passed over the coast, but the most intense winds remained offshore.

The QuikSCAT observation of Ophelia shown at 25 km and 2.5 km resolution in Figs. 3.17a and 3.17b respectively occurred just before the storm reached peak intensity for the second time. The NHC best-track is plotted in Fig. 3.16. Along the best-track in this plot, the circle indicates the location of the QuikSCAT observation taken from rev 32493 on 14 September 2005 at 23:07 UTC. The black region in the north-west of the wind field images is North Carolina. The grey represents the near-coastal exclusion masks for each resolution. The mask for standard resolution wind

44
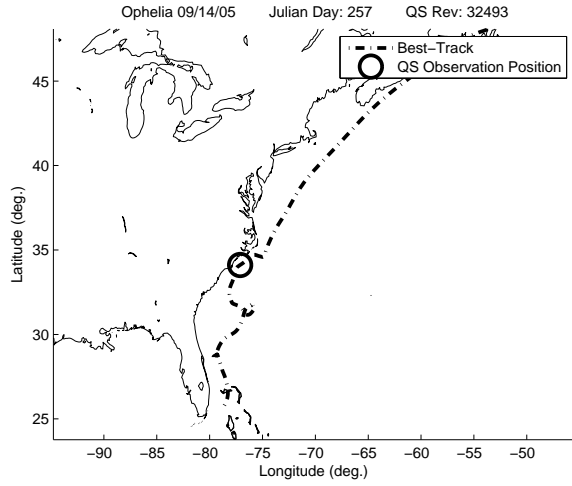
Figure 3.16: National Hurricane Center Best Track for Hurricane Ophelia (2005)

retrieval in Fig. 3.17a extends further from the coast than the mask for ultra-high resolution wind retrieval. This affords observation of a larger portion of the storm—particularly its core—in the resolution enhanced wind field.

Comparing Fig. 3.17a with Fig. 3.17b, the same general wind field is recognized in each. Note that the wind direction vectors in this observation do not exhibit the expected vorticity in the core of the storm. This is likely due to ambiguity selection errors. Examining the wind speed field at the two resolutions, it is difficult to estimate the size of the storm's eye and how much of it is over land. The standard resolution near-land mask extends to cover part of the storm's core. Additionally, at 25 km resolution, the relatively small eye is not viewed in sufficient detail to infer its size, structure, and precise location. With the 2.5 km wind speed field, nearly the entire eye is visible. Precise identification of the storm center is possible. The northern portion of the eyewall is seen passing over the coast, while the calm eye remains off shore. Somewhat faint rain bands are visible to the east of the storm's core.

Observing Hurricane Wilma at landfall on the Yucatan Peninsula shows similarly added detail and coverage in the enhanced resolution wind field. Wilma was one of the most intense Atlantic hurricanes on record. The lowest central pressure ever recorded in an Atlantic hurricane (882 mb) occurred in Wilma while at peak

45
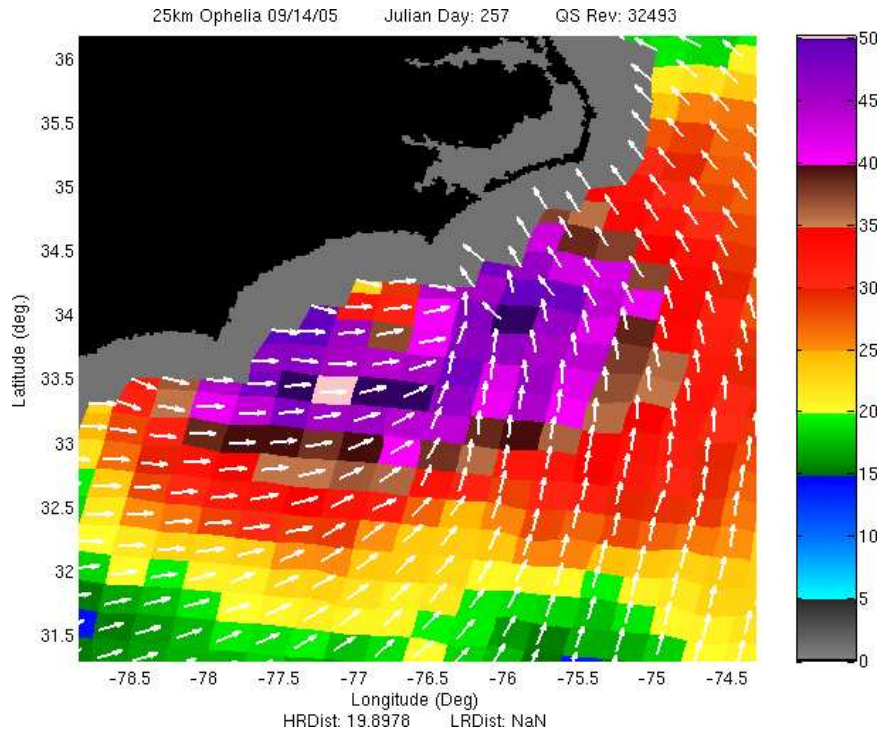
(a)
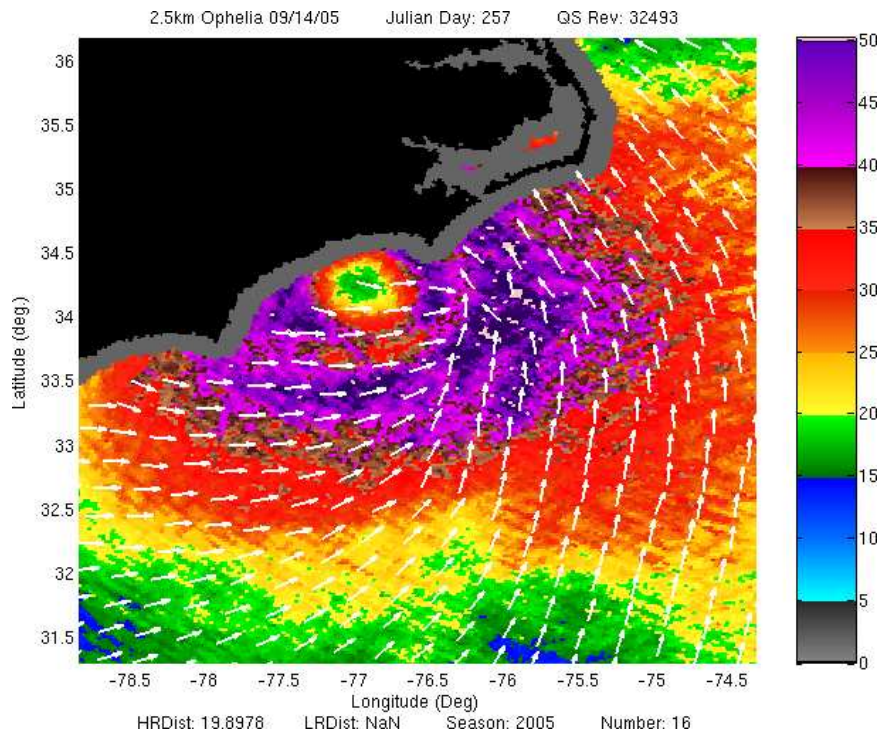
(b)

Figure 3.17: Structure of Hurricane Ophelia near land in 2005
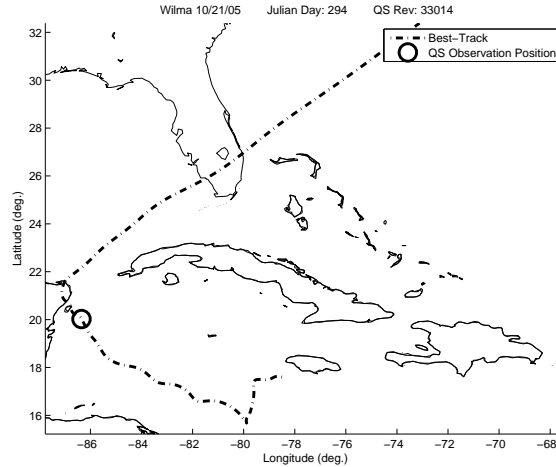
Figure 3.18: National Hurricane Center Best Track for Hurricane Wilma (2005).

intensity [25]. It was a large storm and made landfall twice—first on the Yucatan Peninsula and then in Florida. Its landfall can be seen in Fig. 3.18, the NHC best-track of Wilma's path. Hurricane Wilma's intensity, size, and path resulted in a wide swath of severe damage. Twenty-two deaths were directly attributed to Wilma in Haiti, Jamaica, Mexico, and Florida. Wilma also caused the largest electrical service disruption ever in Florida with up to 98 percent of South Florida without power. In the United States alone, the damage estimates due to Wilma are estimated to be $12.2 billion [25]. Detailed information about damage in Mexico is not available.

In Fig. 3.19, we observe Hurricane Wilma affecting the eastern edge of Mexico's Yucatan Peninsula. QuikSCAT rev 33014 observed Wilma on 21 October 2005 at 11:26 UTC just as it was reaching the island of Cozumel. The location of this observation is indicated by the circle in Fig. 3.18. At the time, Wilma was still a very intense Category 4 with NHC estimated maximum winds of 130 kt. It would weaken slightly as it crossed Cozumel, but remain a major hurricane at Category 4 upon landfall on the mainland Yucatan. Figure 3.19a shows the L2B wind field for the QuikSCAT observation of Wilma described above. The Yucatan peninsula is represented by the large black region in the northwest corner of the image. Cozumel is the large island just offshore at approximate lat/lon coordinates of 25.5 N, -87 E. The

near-to-land mask is shown as the light grey regions bordering the black land masses.

The wind direction field in the standard resolution wind field image shows evidence of ambiguity selection errors as there are several inconsistent wind directions within the field—especially near the center of the storm. In the direction field, the general circulation remains observable despite the ambiguity selection errors. Still, determining the precise location of the circulation center is somewhat ambiguous in the L2B direction field. Examining the L2B wind speed field, a high retrieved wind speed core is clear. Several WVCs with wind speed in excess of 50 kt are present within this core. Ambiguity remains, though, in determining the circulation center and the structure of the storm's core. Additionally, it is difficult to determine exactly which part of the storm lies within the near-to-land mask.

Observing at 2.5 km resolution (Fig. 3.19b), the structure of the storm is more evident. This figure is plotted as in Fig. 3.19a, but with the enhanced resolution wind speed field. A prominent eye surrounded by an intense, circular eyewall is found just to the southwest of Cozumel. Ultra-high resolution QuikSCAT also reveals that Wilma exhibits dual eyewalls at this stage. The secondary eyewall is seen as a mostly indigo and light pink ring around the obvious inner eyewall. Note that evidence for this secondary eyewall is implied in the standard resolution figure. Indigo regions surrounding the light pink core in the 25 km image co-locate with the secondary eyewall in the 2.5 km image. These regions are not as easily, nor as confidently, interpreted as a secondary eyewall at standard resolution as they are at enhanced resolution.

The difficulty in determining, at standard resolution, the precise geographical location of the storm's structural features is somewhat alleviated at enhanced resolution. Because of the clarity of the primary eyewall, visual extrapolation of the eyewall arc across the near-to-land mask indicates that the northwestern portion of the primary eyewall is just impacting the southeastern coast of Cozumel. Interior to the primary eyewall, a circular area of lower wind speed indicates the hurricane eye. From this observation, we can estimate the location of the storm's circulation center to be the center of the depicted eye. Identification of the circulation center in the

48

standard L2B wind field for this case is more uncertain. In Chapter 4, we specifically consider the differences in identifying tropical cyclone circulation centers at standard and enhanced resolution. Occasionally a circulation center is readily apparent in neither the standard nor the enhanced resolution wind field. Section 3.4.4 looks at this situation and the conditions in which it occurs.
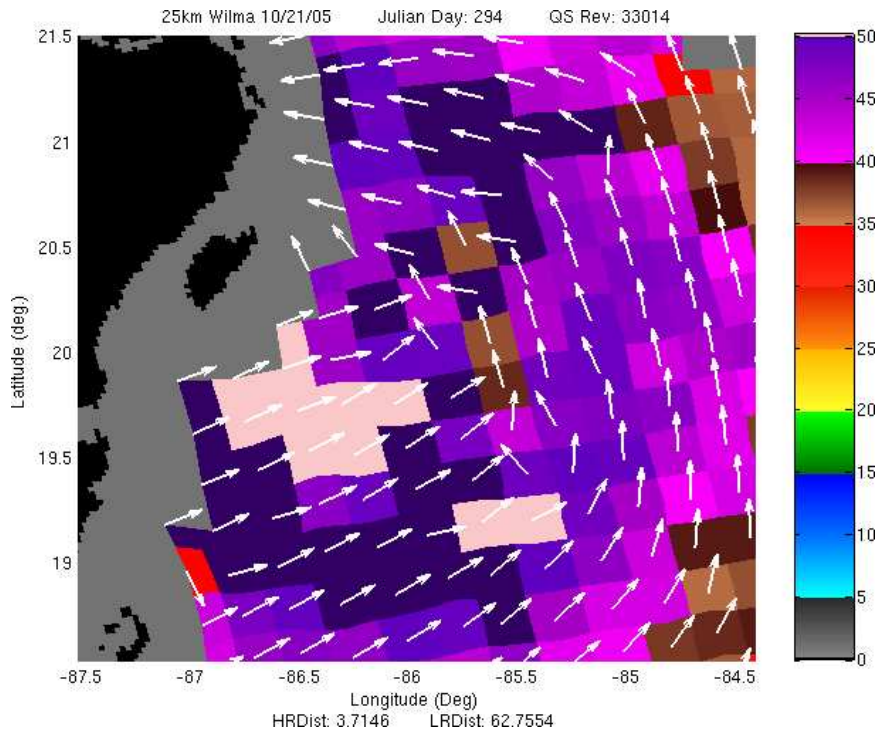
(a)
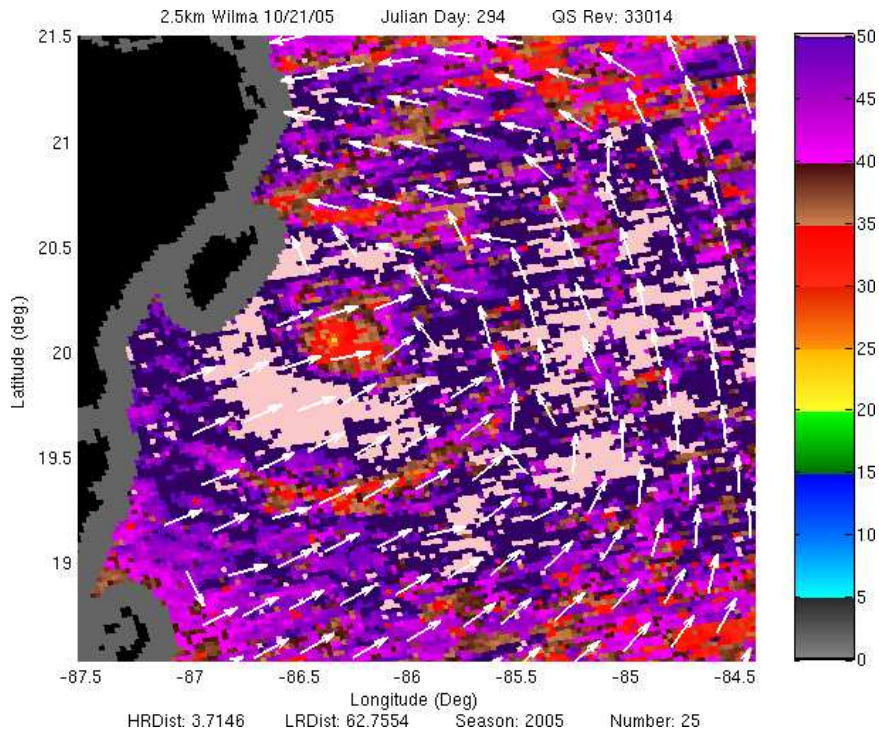
(b)

Figure 3.19: Structure of Hurricane Wilma near land in 2005

3.4.4 Ambiguous Circulation Center

Accurate interpretation of QuikSCAT retrieved wind fields is an acquired skill. Especially for tropical cyclones, a degree of experience is required to infer the true near-surface wind field from the nuanced QuikSCAT retrieval. In considering the utility of resolution enhanced wind fields, we do so from the perspective of one who is familiar with the sensor and its limitations, but perhaps not a seasoned expert in its interpretation. This section illustrates some of the conditions under which enhanced resolution wind speed fields may not contribute significantly to the understanding of a storm's structure for such an individual. It also introduces Chapter 4 by demonstrating some of the considerations and challenges in identifying tropical cyclone circulation centers using QuikSCAT. To that end, we explore QuikSCAT observations of four storms in which cyclonic structure determination is essentially equivalent in both 25 km and 2.5 km wind field images. Most cases entail storms before undergoing much intensification and which range from Category 2 hurricane to tropical storm. As mentioned in Section 2.1.1, tropical storms begin to develop the distinctive cyclonic shape, but generally do not exhibit eyes.

Hurricane Charley was the second major hurricane of the 2004 season. It made landfall in Florida as a Category 4 hurricane after affecting areas of Cuba, Jamaica, and the Cayman Islands. Charley was directly responsible for 10 deaths and an estimated $14 billion damage in the United States. Its path is shown in the best-track plot in Fig. 3.20. The circle represents the location of its observation near the Cayman Islands by QuikSCAT rev 26811 at 10:47 UTC on 12 August 2004. Figure 3.21 shows the wind field for this observation of Charley. At the time, Charley was undergoing a process of intensification. It had reached Category 1 hurricane status earlier on 11 August after approaching Jamaica. By 15:00 UTC 12 August, it was classified as Category 2 on the Saffir-Simpson Hurricane Scale [26].

In the standard resolution wind field (Fig. 3.21a) from QuikSCAT rev 26811, much of the storm's core is obscured by the Cayman Islands and the near-to-land mask. The center is somewhere near the Little Cayman and Cayman Brac Islands, but the extent to which the eyewall occurs over land and the precise location of the
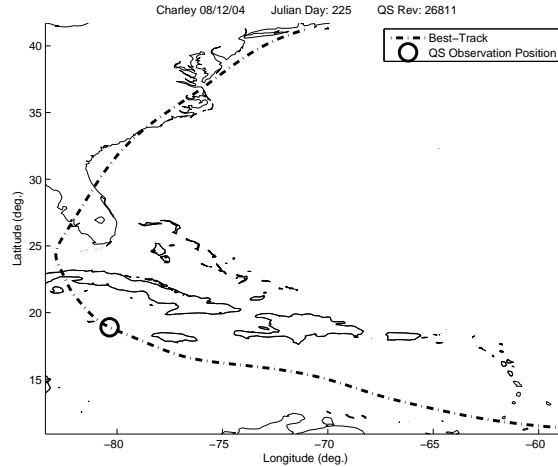
Figure 3.20: National Hurricane Center best-track of Hurricane Charley (2004)

circulation center remain uninferable. Additionally, the wind direction field shows no clear vortex from which the circulation center may be identified.

The enhanced resolution wind speed field in Fig. 3.21b shows somewhat more detail than the standard resolution wind speed field. The overall structure of the storm is more apparent, and rain bands at the fringe of the storm are clear. Still land and the near-to-land mask conceal portions of the storm's core. Examining this wind speed field, though, it is likely that even without the land mask gaps a clear eye would remain unresolvable. The NHC best track places the circulation center of the storm southeast of Grand Cayman at lat/lon about 18.9 N, -80.35 E. There is little evidence in either the 2.5 or 25 km wind fields to place the circulation center there.

Throughout its existence, Charley's eyewall was exceptionally small. Just before its landfall in Florida on 13 August, its eye was estimated to be just 6 nautical miles in radius. This small size is perhaps a factor in the unidentifiability of Charley's circulation center.

The tropical depression that would become Hurricane Erin formed from a tropical wave west of the Cape Verde Islands on 1 September 2004. By the next day it had organized into a tropical storm. Erin would cycle in intensity several times and on 9 September reach peak intensity of 105 kt warranting a Category 3 classification
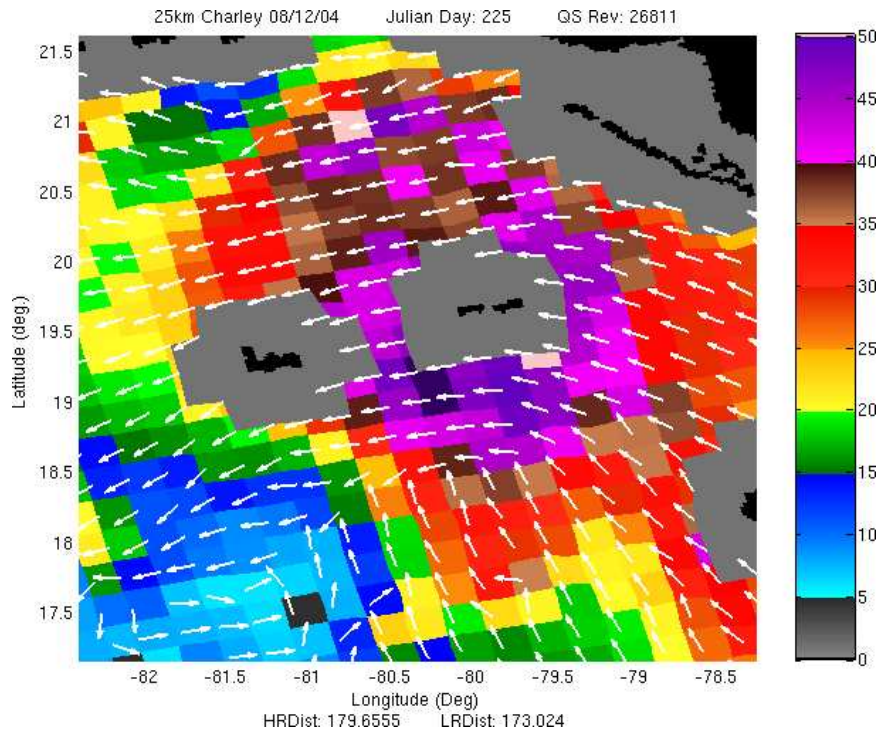
(a)
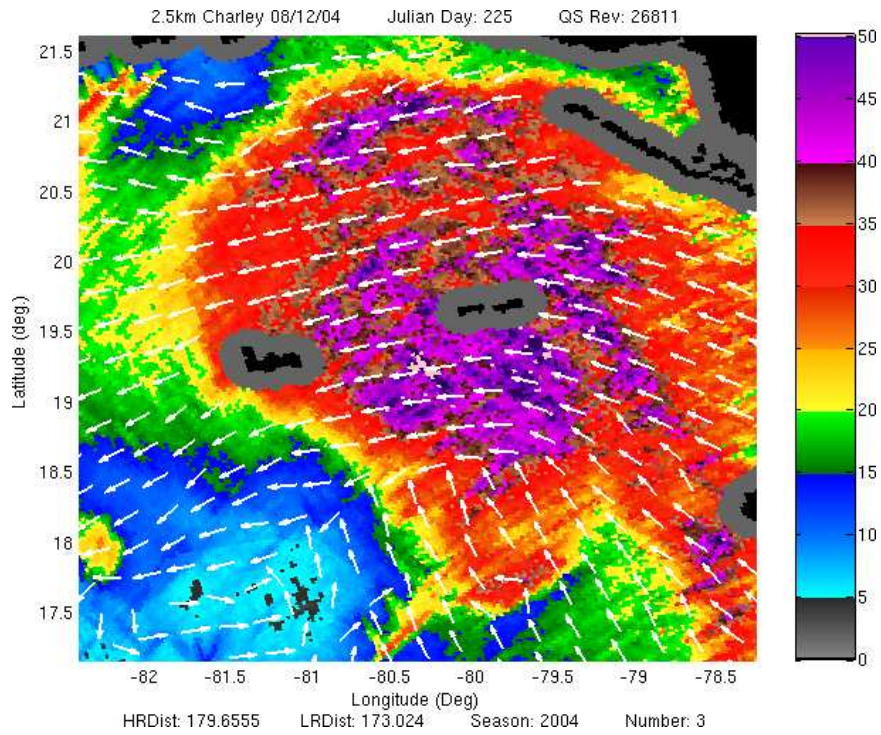
(b)

Figure 3.21: Hurricane Charley with unresolvable eye in standard resolution (a) and ultra-high resolution (b)
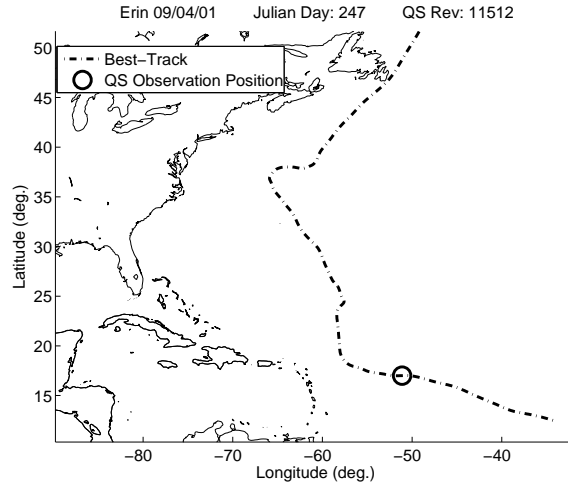
Figure 3.22: National Hurricane Center best-track for Hurricane Erin (2001)

[27]. On 4 September at 09:09 UTC, QuikSCAT rev 11512 observed Erin—then a tropical storm. It had recently lost some of its intensity that was reported to be near 50 kt on 3 September, but was re-strengthening slightly .

Viewed at standard resolution in Fig. 3.23a, it is clear that Erin represents a region of active weather. Several WVCs display wind speed in excess of 40 kt. Within the wind direction field there are evidences of almost closed circulation. Still, a clear circulation center is prominent in neither the wind direction nor the wind speed field. The substitution of the enhanced resolution speed for the standard L2B speed field as in Fig. 3.23b, produces little additional insight. Three small areas of intense wind speed are seen in the northeastern quadrant of the image, but there is not much cyclonic structure in the speed field. Besides the L2B wind direction field, the main indication of circular organization is present in rain bands at the fringes of the storm. They are not sufficiently developed, however, to infer a circulation center. That a clear circulation center remains imperceptible in both wind speed fields is, in this case, perhaps due to the absence of cyclonic circulation in the storm itself. The National Hurricane Center report strengthens this possibility as it indicates that shortly after this observation Erin would degenerate into simply an "area of disturbed weather" before redeveloping and intensifying into a Hurricane[27].

(a)

(b)
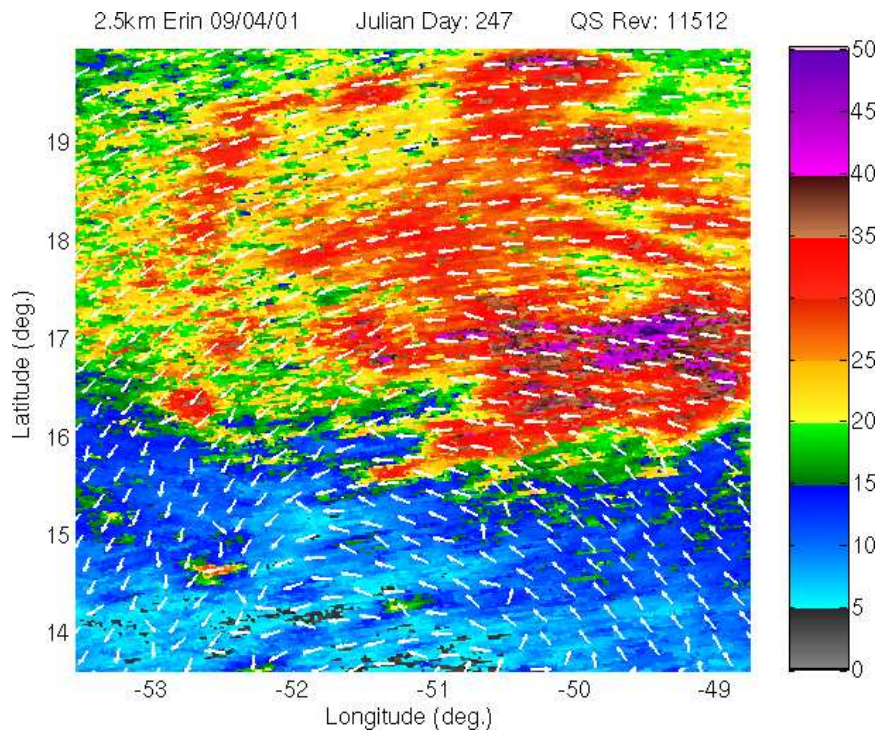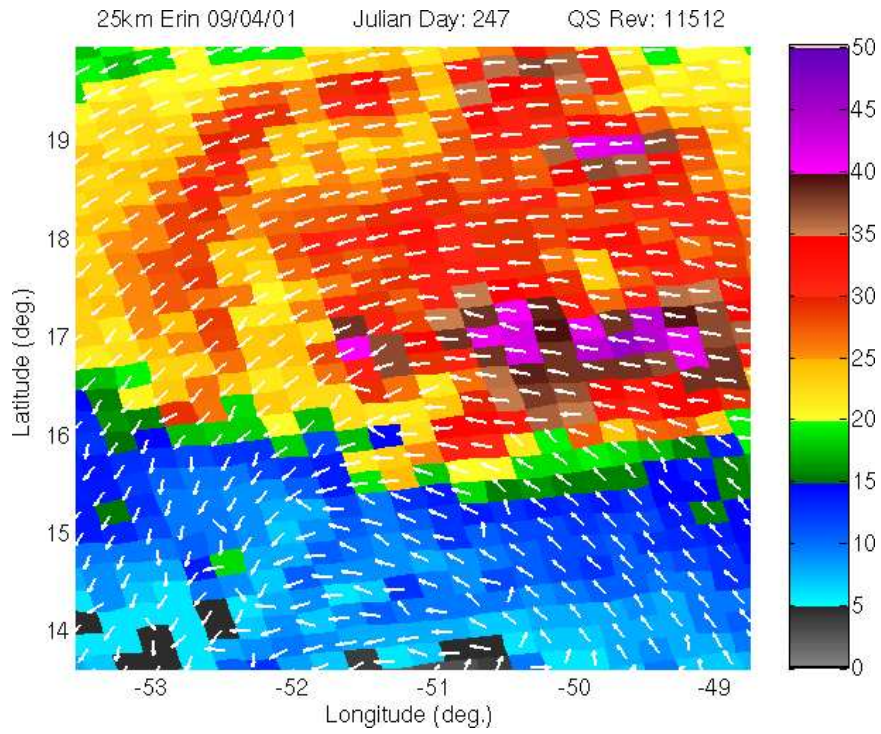
Figure 3.23: Hurricane Erin (as a tropical storm) without a clear circulation center. (a) standard resolution (b) ultra-high resolution
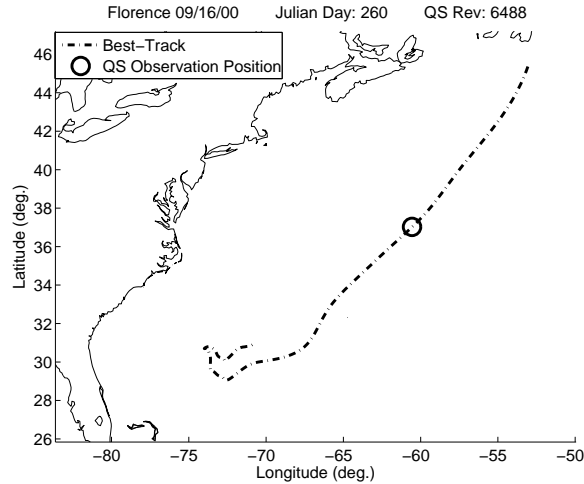
Figure 3.24: National Hurricane Center best-track for Hurricane Florence (2000)

Hurricane Erin was presented in its formation stages well prior to peak intensity, we now consider Hurricane Florence observed near the end of its life as it was beginning to deteriorate. Florence formed subtropically about 600 km west of Bermuda. It reached tropical storm strength at 12:00 UTC on 11 September 2000 and continued strengthening becoming a Category 1 hurricane by 18:00 UTC the same day. Along its northeast path, Florence fluctuated two more times between tropical storm and hurricane. The final transition from hurricane to tropical storm occurred at 00:00 UTC on 17 September. During this transition, at 22:07 UTC on 16 September, QuikSCAT rev 6488 observed the weakening cyclone. The location of this observation is indicated by the circle along the NHC best-track plot in Fig. 3.24.

In the standard resolution wind field of Fig. 3.24a, a clearly closed circulation is present in the wind direction field. The center of vorticity in the wind direction field lies at approximate coordinates -61.5 E, 37.4 N. In the wind speed field, just east of this circulation center, resides a large area of intense wind speed. This region does not wrap around the circulation center, but remains an isolated high wind speed cell. Within the speed field itself, there is little indication of where to place the circulation center. Within the enhanced resolution wind speed field (Fig. 3.24b), there is similarly little evidence for circulation center placement. The primary difference

in the structure of the ultra-high resolution wind speed field is a cluster of several elements retrieved with wind speed in excess of 50 kt. Also, the intense wind speed cell seen in the standard resolution image exhibits more apparent curvature along its outer edge. The center of curvature of this edge co-locates roughly with the circulation center derived from the wind direction field, but the storm center derived from the wind direction field is more obvious. The use of the enhanced resolution wind speed field, in this case, adds only a small amount of confidence to an estimate of the circulation center location. In Chapter 4 we attempt to quantify the added cyclone structure detail obtained through ultra-high resolution wind retrieval by analyzing the accuracy of circulation center placement with standard and enhanced resolution wind fields.
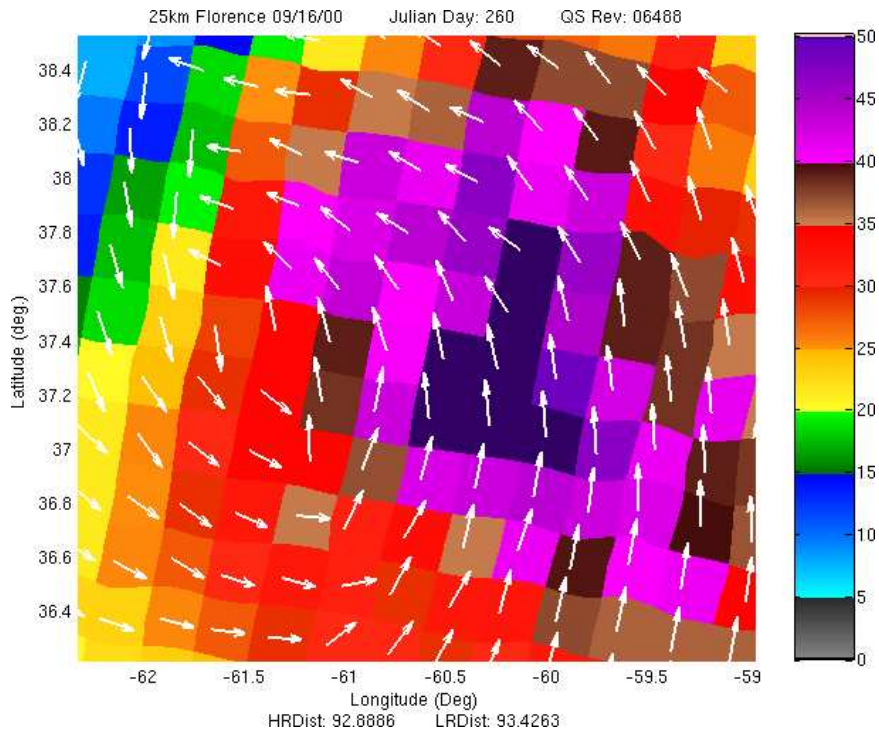
(a)
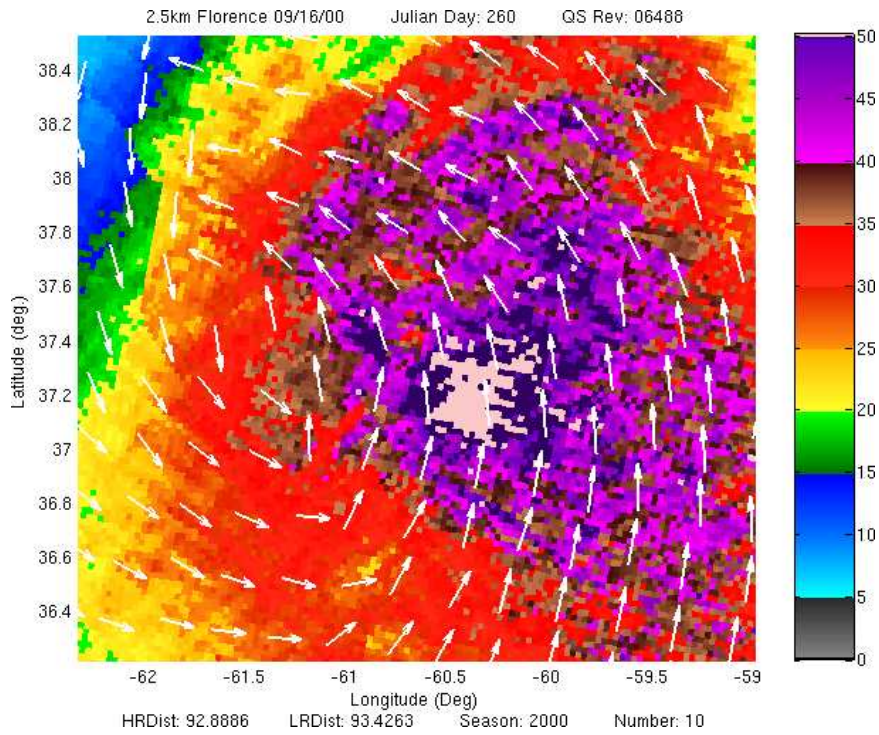
(b)

Figure 3.25: Hurricane Florence with a circulation center in the wind direction field, but no clear eye in the wind speed field. (a) standard resolution (b) ultra-high resolution

58

Chapter 4

Tropical Cyclone Circulation Center Identification

One of the crucial pieces of tropical cyclone information for weather forecasters is an accurate circulation center fix. In order to obtain reliable position fixes, a number of resources are employed including active and passive satellite data in the microwave, visible, and IR spectra; visual, radar, and GPS dropsonde observations from planes; sightings from ships; and surface-based doppler radar information. QuikSCAT is among the active spaceborne sensors used, though most forecasters currently rely on its standard 25 km resolution data. In this chapter, we explore the utility of QuikSCAT data at 25 and 2.5 km posted resolutions for tropical cyclone center identification by comparing perceptible storm center locations at each resolution with the true center fix.

This comparison utilizes QuikSCAT passes observing storms for the tropical cyclone basins adjacent to the United States mainland and all storm seasons over six years of the mission—1999 through 2005. In total, 2513 QuikSCAT observations are used, although not all provide a discernible circulation center because of occlusion by land, an insufficiently developed storm, or poor QuikSCAT coverage. We describe our procedure for circulation center identification illustrated with example center fixes of various conditions and present the results of the locatability analysis.

"Truth data" for circulation centers are from the National Hurricane Center's "best-track" positions. These subjectively smoothed representations of tropical cyclones' locations and intensities are produced at six hour intervals. They are based on post storm analysis of all available data. For more useful comparison, we interpolate the six hour best-track positions using a parametric spline method to QuikSCAT

observation times.

4.1 Center Identification Using Standard and Ultra-High Resolution

Determination of circulation center positions from QuikSCAT winds is done subjectively by observation of the wind speed field at each resolution with the standard-product (L2B) wind direction field overlaid. Resolution enhanced wind directions are noisier than standard resolution wind directions. For this reason, we overlay standard resolution direction vectors onto both the 25 km and the 2.5 km wind speed field.

4.1.1 Method Description

The relative degrees to which the speed and direction fields are utilized in center determination for this comparison vary. At 25 km, we primarily utilize the direction field to locate the circulation center directly. This is complicated, however, because QuikSCAT's sensitivity to rain frequently causes a characteristic pinning of the wind direction field toward the cross-track for severe storms. In such cases, we derive the circulation center from the 25 km speed field alone. The additional detail evident in the ultra-high resolution speed field warrants its increased emphasis in storm center determination for 2.5 km images. To determine the circulation center using ultra-high resolution images, we identify the circular pattern in the wind speed field from the high wind speed eyewall to the relatively calm center. The resolution-enhanced storm center fix is estimated to be at the center of this low speed region.

4.1.2 Example Identifications

The following sections further describe the tropical cyclone circulation center location method used in this study. We present several representative identifications illustrating frequently encountered wind field observation conditions. The conditions presented here are the following: 1) standard resolution identification using the wind direction field, 2) enhanced resolution identification using the wind speed field, 3) identification by standard and enhanced resolution with the wind direction field

pinned toward the cross-track, and 4) unidentifiable circulation centers in standard and enhanced resolution wind fields.

4.1.2.1 Conventional identification using 25 and 2.5 km QuikSCAT winds

In order to determine the circulation center of tropical cyclones using 25 km winds, we plot the standard product (L2B) direction field (small white arrows) overlaid onto the standard resolution speed field as in Fig. 4.1. Represented in this figure is a view from the QuikSCAT standard L2B product of the circulation center of Hurricane Juan, a Category 2 (maximum) hurricane, on September 27, 2003. This figure additionally shows a spline interpolation of the National Hurricane Center best-track (black curve) and the best-track position interpolated to QuikSCAT observation time (black circle). When estimating cyclone circulation centers for this study, the best-track information is not included; it is plotted here for illustrative purposes.

In conventional cases, a circulation center is evident within the QuikSCAT 25 km wind *direction* vectors. It is delineated by the large blue arrow as in Fig. 4.1. The error between the selected center fix and the interpolated best-track position for this case is approximately 84.8 km. This relatively large error results from a significantly displaced circulation center in the L2B wind direction field.

To determine the circulation center of tropical cyclones using ultra-high resolution data, we follow a similar procedure to the standard resolution cases, but substitute the 2.5 km speed field for the 25 km speed field. For reference, we plot standard product direction vectors. These are not used in 2.5 km location of developed storms. Fig. 4.2 shows the same QuikSCAT observation as in Fig. 4.1, but viewed with the resolution-enhanced wind speed field.

Additional storm structure is immediately apparent in the enhanced resolution field in Fig. 4.2. Outer rain bands are clearer, and there is greater wind speed contrast in the eye wall region. The lower wind speed eye is evident.

For conventional cases at ultra-high resolution, the circulation center location is estimated to be the center of the low wind speed area (large blue arrow). For Fig. 4.2, this selection nearly co-locates with the interpolated best-track location
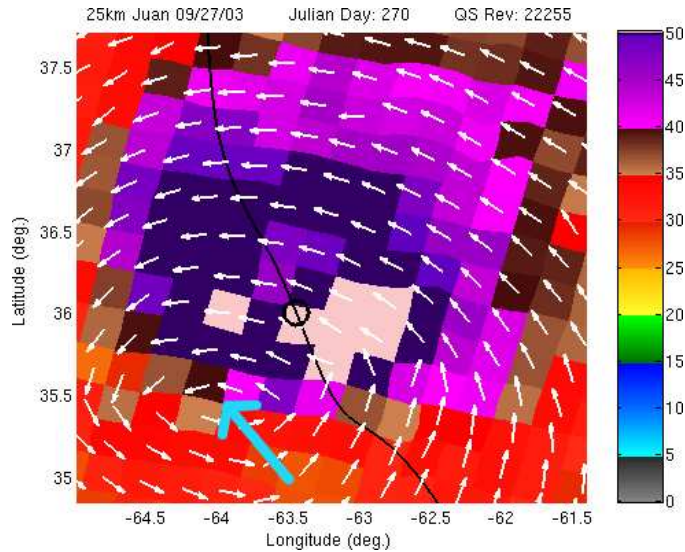
Figure 4.1: QuikSCAT standard resolution observation of Hurricane Juan on September 27, 2003.

(black circle). The error between the storm center selection and best-track is 2.1 km.

4.1.2.2 Rain contaminated (cross-track pinned) case

QuikSCAT is known to be sensitive to rain. Frequently, rain within the measurement swath causes a characteristic bias of the derived wind directions toward the cross-track. As illustrated in Fig. 4.3, a rain-caused cross-track pinning of wind direction combined with the lower resolution speed field leads to difficulty in confidently locating the circulation center of a rain affected storm. This figure shows the standard resolution QuikSCAT observation of Hurricane Michelle, a Category 4 (maximum) storm, on November 2, 2001.

The selected storm center location is again denoted with a large blue arrow. Because of the absence of a discernible vortex in the QuikSCAT direction vectors, the location of this storm center is obtained by roughly identifying the middle of the high wind speed region. There is subjectively greater uncertainty in estimating the circulation center via the standard resolution speed field alone, and the distance to best-track error in this case is 21.4 km.

QuikSCAT retrieved wind speeds are not as sensitive to rain as are wind
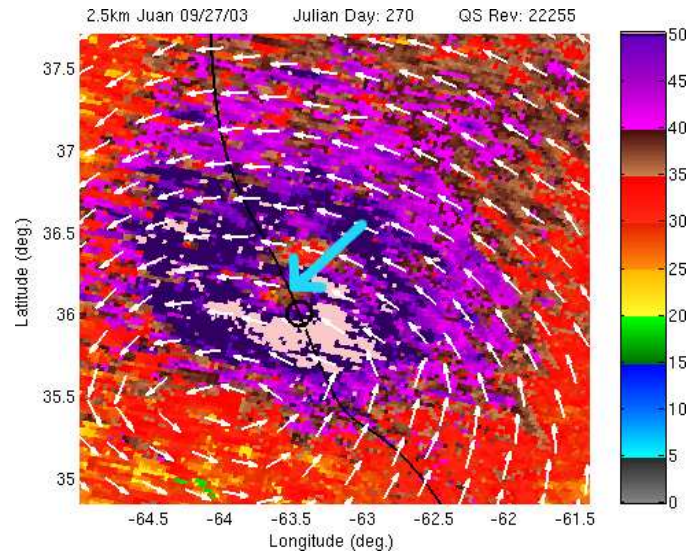
Figure 4.2: QuikSCAT ultra-high resolution observation of Hurricane Juan on September 27, 2003.
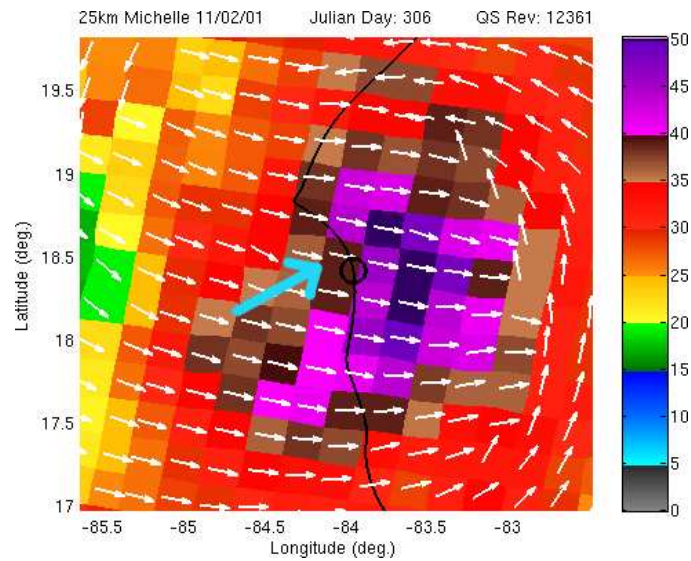
Figure 4.3: QuikSCAT standard resolution observation of Hurricane Michelle on November 2, 2001.
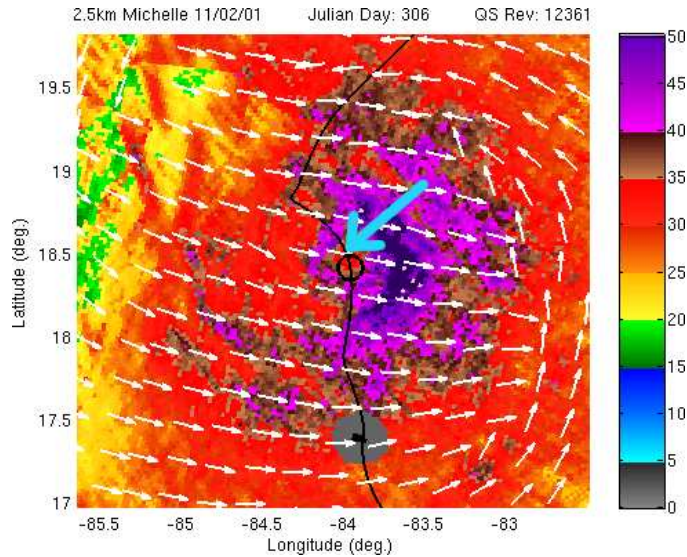
Figure 4.4: QuikSCAT ultra-high resolution observation of Hurricane Michelle on November 2, 2001.

directions. Because of the primary reliance on wind speed, hurricane circulation center location in rain contaminated cases using resolution enhanced winds does not suffer to the same degree from rain-induced wind direction as do standard resolution wind images. As illustrated in Fig. 4.4, the additional storm structure provided by ultra-high resolution wind data enables accurate location of the circulation center even in the absence of meaningful direction information. This image corresponds to the standard resolution observation in Fig. 4.3. The distance from estimated circulation center to interpolated best-track position is 6.2 km. In the following section, we examine center fix accuracy for the data set as a whole.

4.2 Circulation center locatability analysis

This section considers bulk properties of tropical cyclone circulation center identification using standard and enhanced resolution QuikSCAT wind fields. We first describe the data set used herein. Next, we compare sample storm tracks from each resolution against the National Hurricane Center best-track determination. Gross statistics of all circulation center location errors are then presented. We next explore for trends in center fix accuracy correlated to storm basin, maximum sustained wind

speed, and QuikSCAT derived circulation center positions relative to the best-track locations.

4.2.1 Creation of data set

The tropical cyclone data set used herein is comprised of two principal components. First, a global, multi-year set of tropical cyclone best-tracks is searched for co-location with SeaWinds on QuikSCAT. SeaWinds on ADEOS II co-locations are also detected for storms during its mission life. This co-location set includes every QuikSCAT observation of tracked tropical cyclones worldwide from 1999 through 2004. For storms within the Northern Atlantic, Central Pacific, and Eastern Pacific basins, best-tracks are produced by the National Hurricane Center. The co-location data set additionally includes QuikSCAT observations of storms within the 2005 season for these basins. Best-tracks for storms occurring in the Western Pacific, Indian Ocean, and Southern Hemisphere basins are generated by the Navy's Joint Typhoon Warning Center and have not yet been released for 2005 storms.

The co-location set includes the name, basin, season's storm number, maximum sustained wind speed, and calendar date of each storm observation in addition to the QuikSCAT rev number, observation time, and approximate storm location. In all, 6010 storm co-locations are cataloged, though some observations do not spatially cover the entire storm. Ultra-high resolution $\sigma°$ and wind fields are generated for each of these storm co-locations. Additionally, nine standardized .gif images of several scatterometer parameters are created and made available to meteorologists and climatologists via the image archive at NOAA's QuikSCAT storm page: http://manati.orbit.nesdis.noaa.gov/cgi-bin/qscat_storm.pl. The five $\sigma°$ images created include one for each of the four azimuth/polarization combinations (aft-looking horizontally polarized, fore-looking horizontally polarized, aft-looking vertically polarized, and fore-looking vertically polarized) and one for the mean of the four $\sigma°$ values. Two wind barb images are created for each observation: one of all ambiguities in the L2B wind field, and one of the selected ambiguities in the L2B wind field. Two wind field images similar to those used herein are also made available.

The second component of the data set entails the standard and ultra-high resolution derived tropical cyclone center fixes. This requires examining the wind field images for every co-location and at each resolution for the presence of an identifiable circulation center. We performed this for all observations within the two basins directly affecting the United States mainland—the Northern Atlantic, and Eastern Pacific. In total, 2513 partial or total storm observations were examined within these two basins. Circulation centers were identified in 1512 enhanced resolution observations and in 1298 standard resolution observations. They were identified at both resolutions simultaneously in 1222 co-locations. Circulation centers were identifiable in 214 more cases at enhanced resolution. Appendix A includes additional details regarding the tropical cyclone co-location data set and software tools developed for its creation.

4.2.2 Bulk error analysis

In addition to having a greater number of identifiable circulation centers, ultra-high resolution wind fields identified centers with smaller mean error. From the 1222 observations in which a circulation center was identified in both the standard and ultra-high resolution wind fields, the mean distance to the interpolated best-track position (error) is 48.2 km and 38.5 km respectively. The standard deviations of error are roughly the same at 40.9 km and 39.3 km respectively. Error histograms of this set are plotted for standard (Fig. 4.5) and enhanced (Fig. 4.6) resolutions.

Over each histogram, a gamma distribution, $\Gamma(k, \theta)$, is plotted. The gamma distribution parameters are selected to be 2 and $\overline{error}/2$ for the shape (k) and scale (θ) respectively. We surmise that the excellent fits achieved using these parameters arises out of the nature of the underlying random variables.

If we assume that the positions of both the best-track and the QuikSCAT derived locations relative to the true circulation center are independently Gaussian in latitude ($\Delta Lat \sim N(0, \sigma^2)$) and longitude ($\Delta Lon \sim N(0, \sigma^2)$) then the magnitude of each error can be expressed as

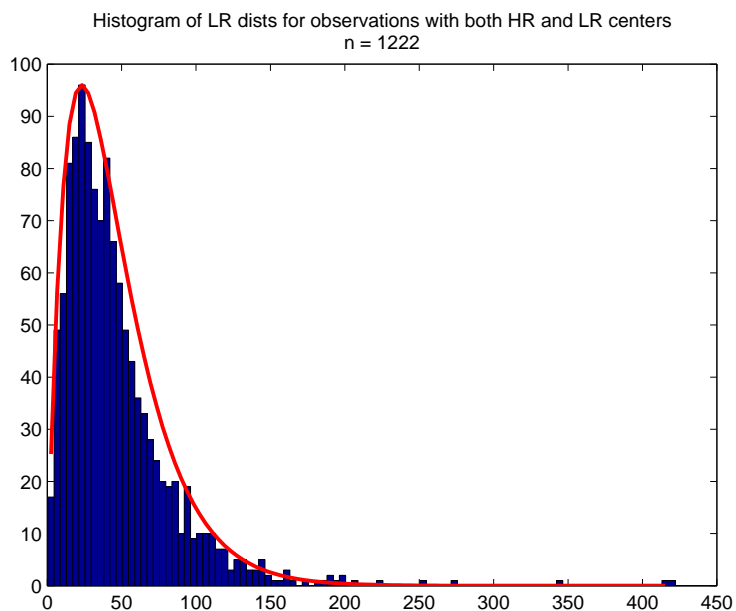$$\sqrt{\Delta Lat^2 + \Delta Lon^2} \sim Rayleigh(\sigma).$$

Figure 4.5: Histogram of distance (km) from standard resolution center fixes to interpolated best-track location (error) for all storm basins.
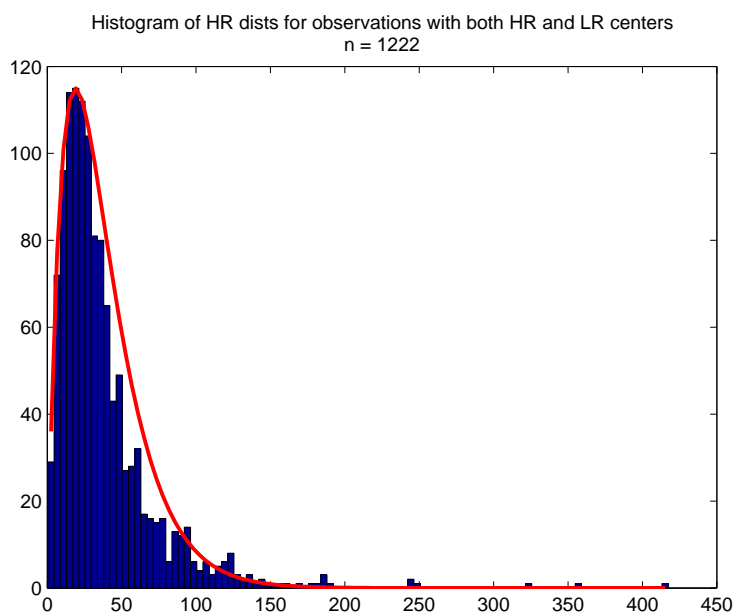

Figure 4.6: Histogram of distance (km) from enhanced resolution center fixes to interpolated best-track location (error) for all storm basins.

The "error" from best-track to QuikSCAT derived center is then related to the sum of square of the two Rayleigh distributed errors,

$$Rayleigh^2(\sigma) + Rayleigh^2(\sigma) \sim \Gamma(2, 2\sigma^2).$$

In order to match the mean of this distribution ($k\theta$) to that of the histogram data, we set the scale parameter (θ) equal to the one-half the average error for each resolution and plot the properly scaled $\Gamma(2, \overline{error}/2)$ distribution. This fits remarkably well to the error histograms.

Besides the overall accuracy improvements, when performing tropical cyclone center fixing, we had subjectively higher confidence in individual circulation center identifications using enhanced resolution as compared with the same identifications using standard resolution. This is demonstrated by the error in observations for which a circulation center was identified in only a single resolution wind field—either standard or enhanced resolution. The difference in number alone suggests a higher analyst confidence. Enhanced-resolution-only identifications totaled 290 compared with 76 for standard-resolution-only.

The error histograms in Fig. 4.7 (standard-resolution-only) and Fig. 4.8 (enhanced-resolution-only) further emphasize the increased analyst confidence. The mean error for enhanced-resolution-only identifications, 47.53 km, is somewhat higher than the 38.5 km mean for all enhanced resolution cases. Still, it is significantly lower than the average error for standard-resolution-only identifications, 74.8 km. That both the number and accuracy of enhanced-resolution-only center fixes are higher than those of standard-resolution-only center fixes suggests that the analyst is more able to differentiate identifiable from non-identifiable circulation centers using the resolution enhanced wind fields.

4.2.3 Error by basin

When observing center fix errors by basin, the general trends remain. Ultra-high resolution circulation center locations are, on average, closer to the interpolated best-track location. Figures 4.9 and 4.10 plot the center fix error for the Northern

Figure 4.7: Histogram of distance (km) from enhanced resolution center fixes to interpolated best-track location (error) for circulation centers only identifiable in standard resolution wind fields.
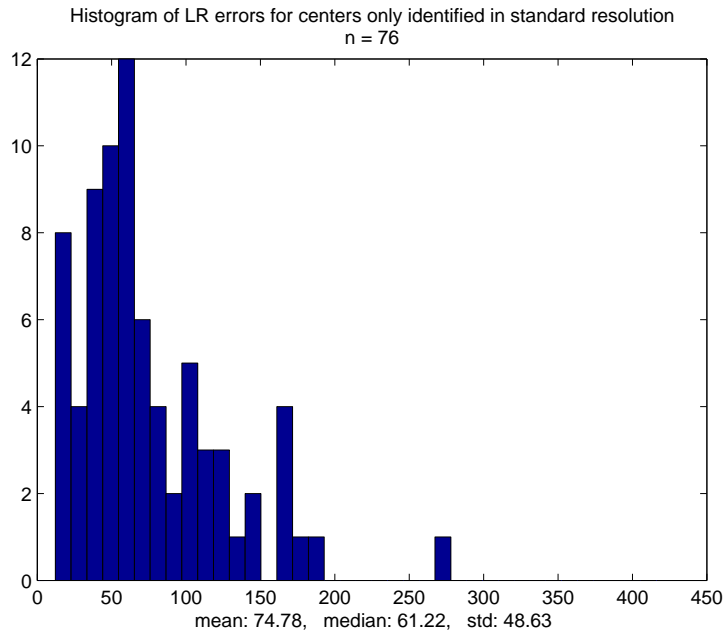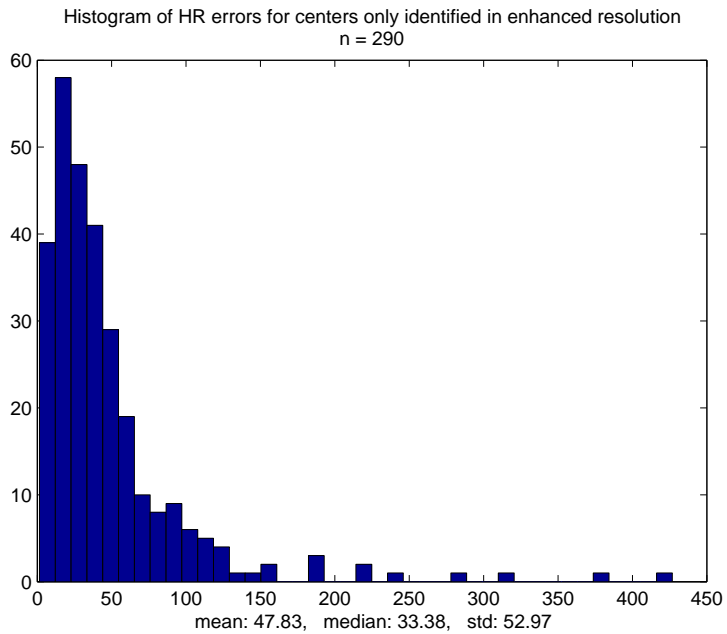

Figure 4.8: Histogram of distance (km) from enhanced resolution center fixes to interpolated best-track location (error) for circulation centers only identifiable in ultra-high resolution wind fields.

Figure 4.9: Histogram of distance (km) from standard resolution center fixes to interpolated best-track location (error) for the Northern Atlantic storm basin.

Atlantic basin at standard and enhanced resolutions respectively. Similarly, Figs. 4.11 and 4.12 do so for the Eastern Pacific basin. We observe that the average errors in the Eastern Pacific basin are somewhat lower than those of the Northern Atlantic basin. This is probably due to the smaller average size for Eastern Pacific storms resulting in a smaller region of possible mis-location error. There was no perceptible trend when controlling for observation latitude and longitude.

4.2.4   Error by wind speed

More developed storms—or ones with higher wind speeds—are expected to have a more clearly defined eyewall and, consequently, to be more easily located. Figures 4.13 and 4.14 represent the error in center fixes plotted according to the NHC maximum sustained (1 min) wind speed. For standard resolution circulation center locations, there is not much of a trend associated with maximum sustained wind speed. On average, there is a slight improvement in enhanced resolution center fixes with increased wind speed.
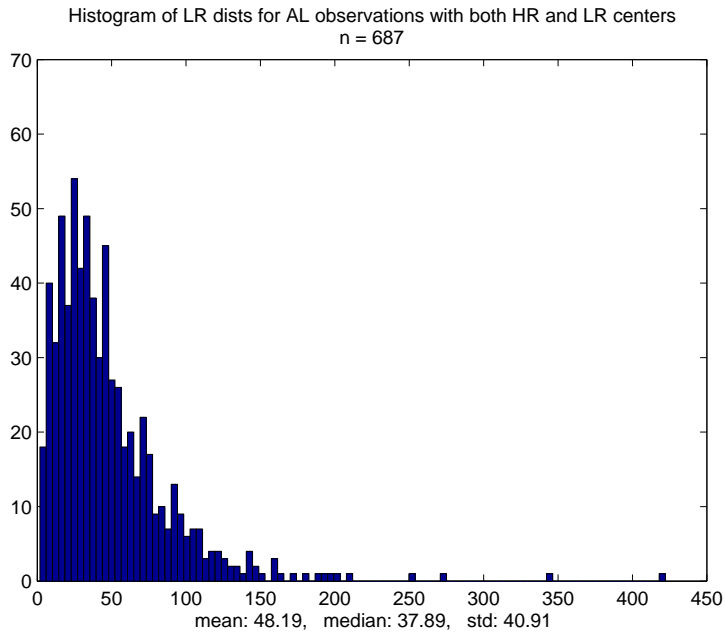
70

Figure 4.10: Histogram of distance (km) from enhanced resolution center fixes to interpolated best-track location (error) for the Northern Atlantic storm basin.

Figure 4.11: Histogram of distance (km) from standard resolution center fixes to interpolated best-track location (error) for the Eastern Pacific storm basin.
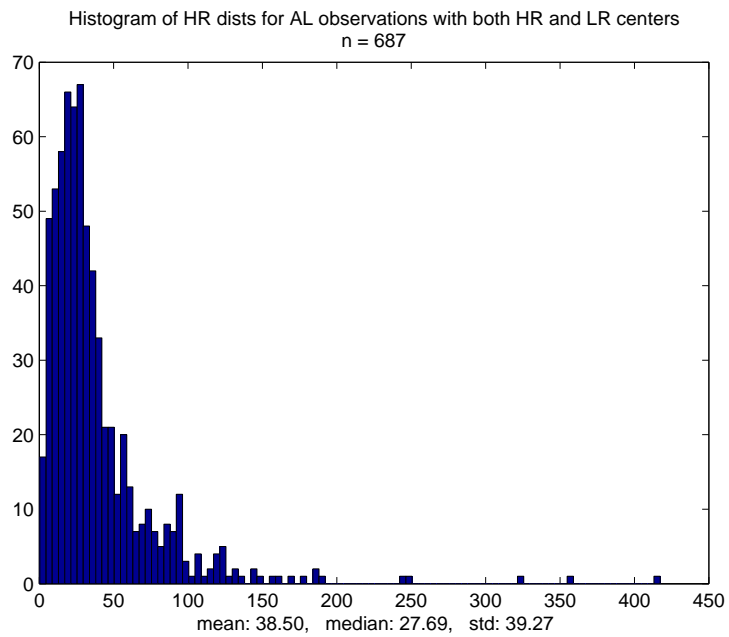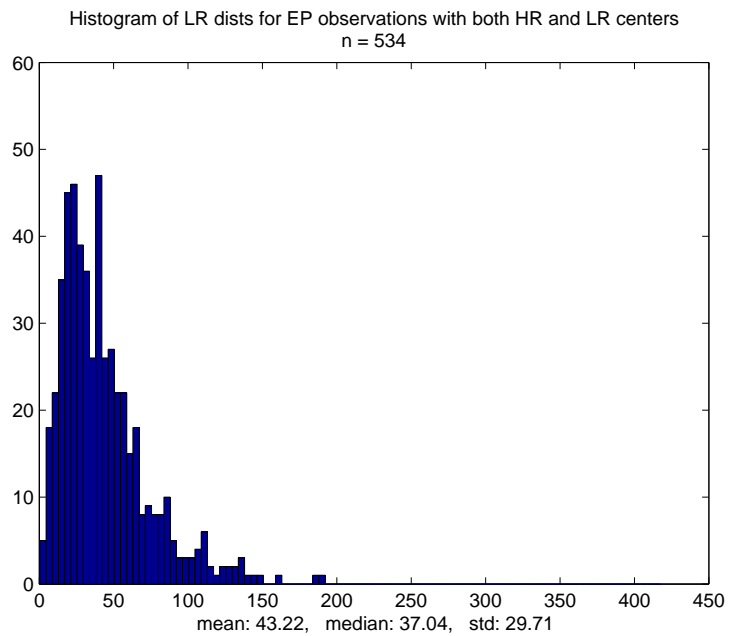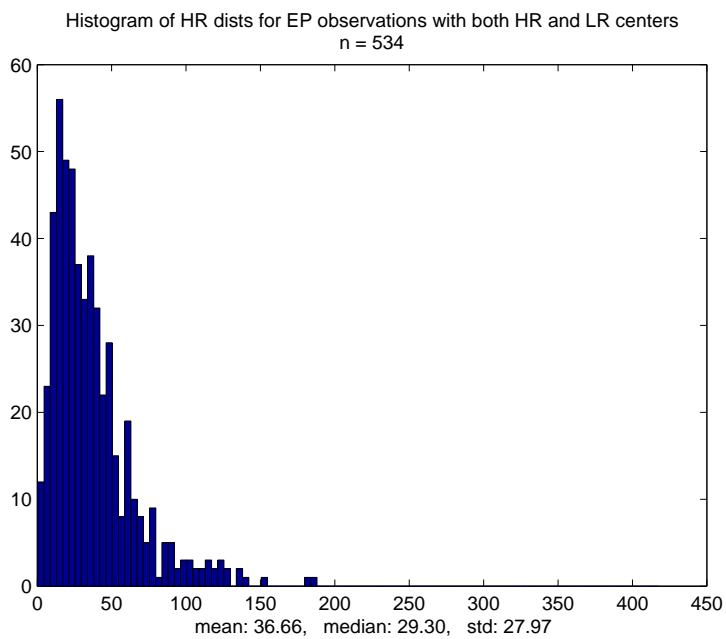
Figure 4.12: Histogram of distance (km) from enhanced resolution center fixes to interpolated best-track location (error) for the Eastern Pacific storm basin.
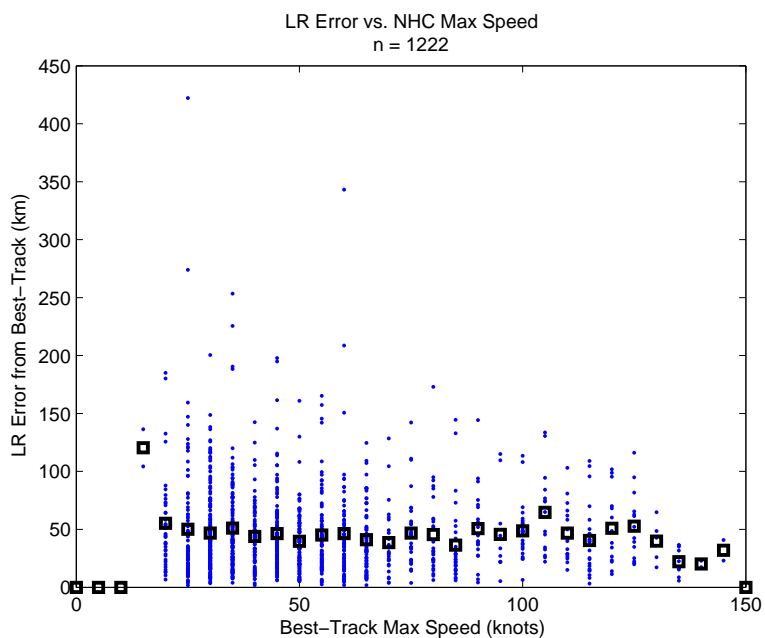
Figure 4.13: Scatterplot of error in standard resolution center fixes vs. best-track maximum wind speed.
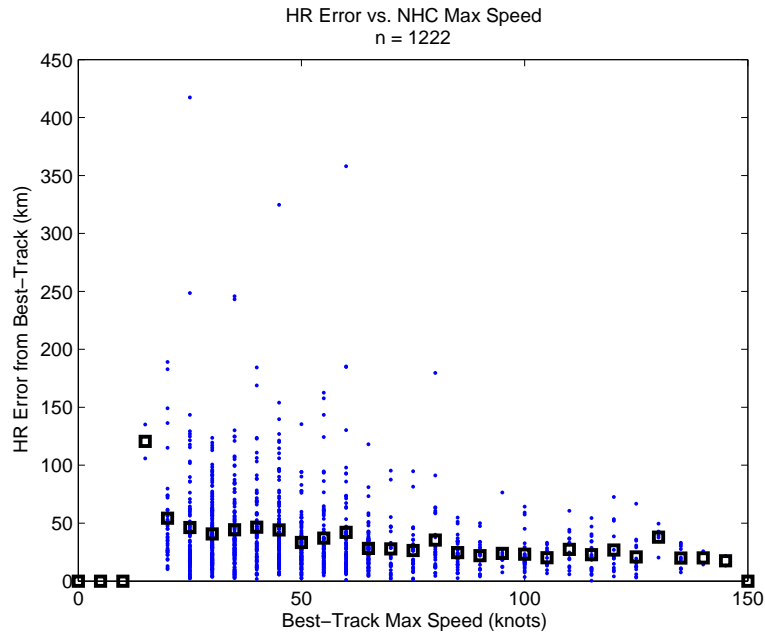
Figure 4.14: Scatterplot of error in enhanced resolution center fixes vs. best-track maximum wind speed.

4.2.5 Error locations relative to best-track

In examining a multitude of QuikSCAT tropical cyclone wind fields, there appeared to be a slight bias to the southwest in the circulation center location. This is perhaps because of the temporally and spatially coarse National Centers for Environmental Prediction (NCEP) model winds used to nudge the QuikSCAT wind field for ambiguity removal. NCEP winds are generated in six hour increments. Within this time period, however, a tropical cyclone may have moved significantly. This displacement in the actual and nudging wind field may be evidenced as a bias in the circulation center location. In order to detect such a bias, we plot the position of the QuikSCAT derived center fixes relative to the actual interpolated best-track positions. These are shown in Fig. 4.15 for standard resolution, and Fig. 4.16 for enhanced resolution. For reference, we also plot cross-hairs at the relative best-track position. In observing these figures, a slight southwesterly bias is apparent. It is more pronounced in the standard resolution position fixes than in the ultra-high resolution fixes. The average offset is approximately 0.14 deg to the southwest for the standard

73

Figure 4.15: Scatterplot of the location of standard resolution center fix positions relative to interpolated best-track locations.

resolution cases and approximately 0.09 deg to the west-southwest for the enhanced resolution cases.

4.2.6 Maximum wind speed comparison

In their best-track data sets, the NHC provides an estimate of the maximum sustained wind speed. This provides an opportunity for comparison with the QuikSCAT retrieved wind fields.

For each tropical cyclone observation, we determine the maximum QuikSCAT wind speed—at each resolution—within a radius of 50 km and 100 km of the interpolated best-track location. We then compare this maximum wind speed to the value reported by the closest (in time) NHC best-track entry. A plot of each QuikSCAT derived maximum wind speed versus the NHC reported value is shown in Figs. 4.17 (standard resolution, 50 km radius), 4.18 (enhanced resolution, 50 km radius), 4.19 (standard resolution, 100 km radius), and 4.20 (enhanced resolution, 100 km radius). The mean QuikSCAT-derived maximum wind speed for each corresponding NHC
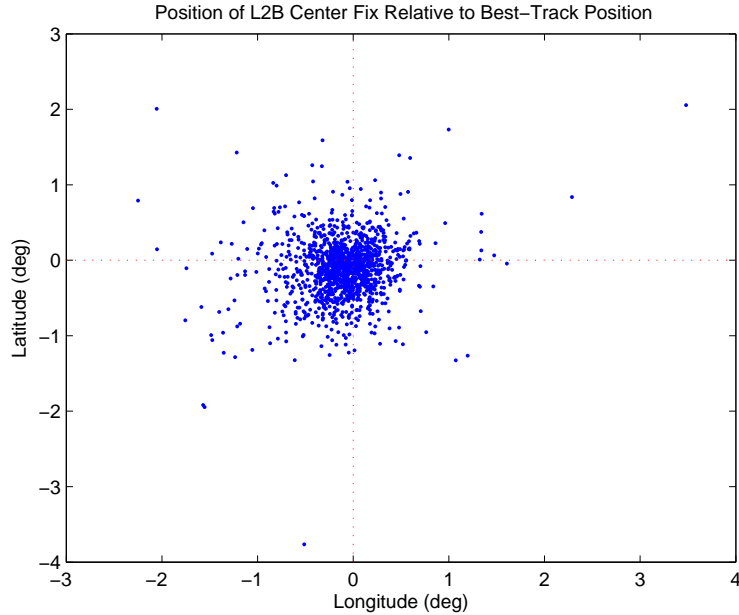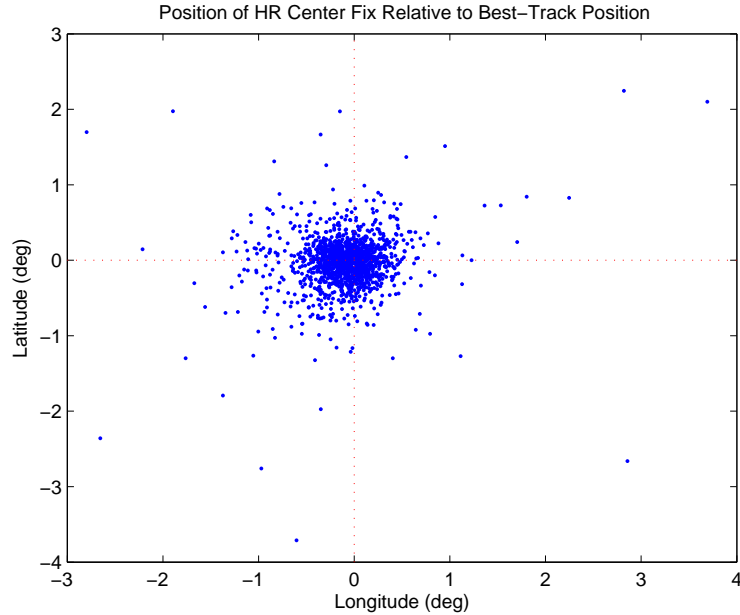
Figure 4.16: Scatterplot of the location of enhanced resolution center fix positions relative to interpolated best-track locations.

maximum sustained wind speed is noted by a black square.

It is important to note that the QuikSCAT derived maximum winds represent an essentially instantaneous observation whereas the NHC reported maximum sustained winds represent a 60 second average. The relation between the instantaneous and sustained maximum wind speeds is termed a gust factor, $G = max_{inst}/max_{sus}$. A generally accepted value for G is 1.3, meaning that instantaneous wind gusts are typically 30% higher than sustained maximum wind speeds [28]. Gust factors vary with a number of parameters including the averaging time, topographics, height, and wind speed, but gust factors on the order of 1.3 are frequently used for 1 min sustained open ocean winds for 10 m above surface retrievals in tropical cyclones.

Within the maximum wind speed figures (4.17 - 4.20), two comparison lines are plotted. The lower (red) line represents the diagonal. The upper (green) line represents the gust factor augmented maximum wind speed. These plots, especially for enhanced resolution, exhibit a maximum wind speed ceiling near 100 knots. This is due to the QuikSCAT geophysical model function's maximum retrievable wind of

Figure 4.17: Scatterplot of the maximum L2B wind speed within a 50 km radius of the interpolated best-track position vs. the best-track maximum sustained (1 min) wind speeds. The mean value at each best-track reported maximum speed is shown with a black square. The diagonal is shown in red, and the gust factor line is shown in green.
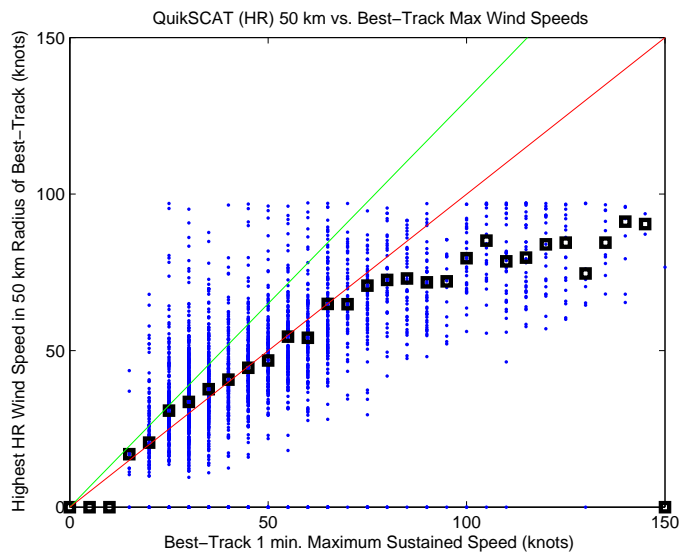
Figure 4.18: Scatterplot of the maximum enhanced resolution wind speed within a 50 km radius of the interpolated best-track position vs. the best-track maximum sustained (1 min) wind speeds. The mean value at each best-track reported maximum speed is shown with a black square. The diagonal is shown in red, and the gust factor line is shown in green.
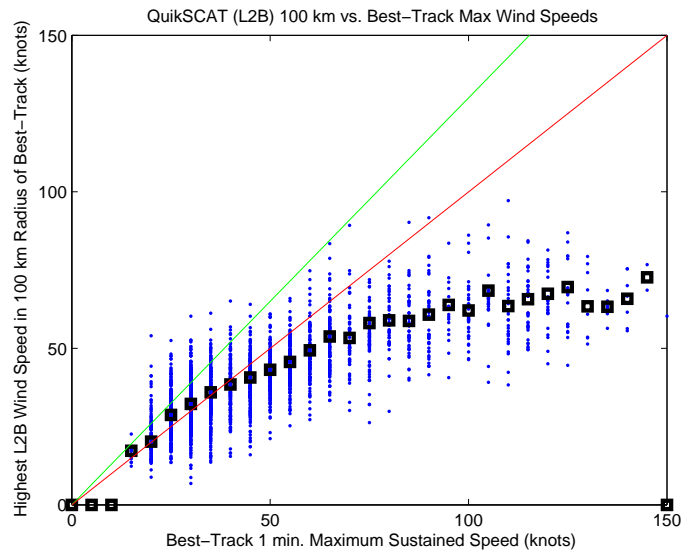
Figure 4.19: Scatterplot of the maximum L2B wind speed within a 100 km radius of the interpolated best-track position vs. the best-track maximum sustained (1 min) wind speeds. The mean value at each best-track reported maximum speed is shown with a black square. The diagonal is shown in red, and the gust factor line is shown in green.
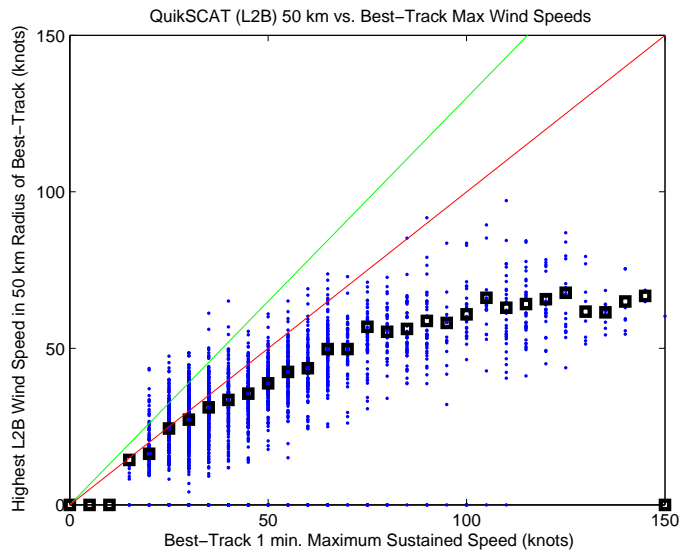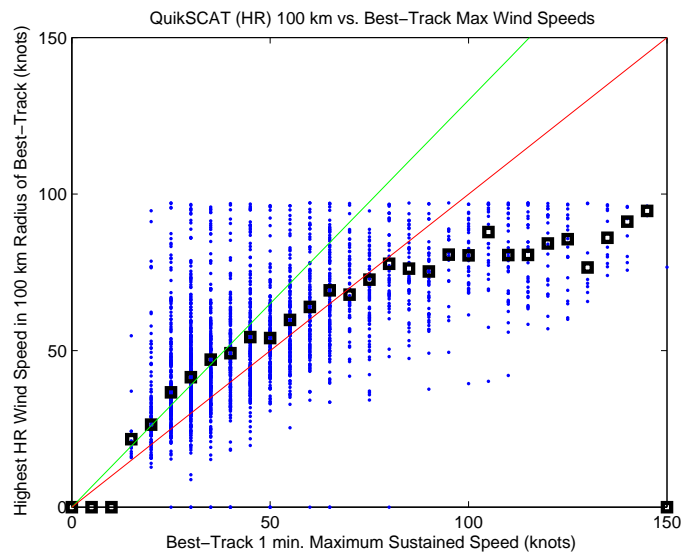

Figure 4.20: Scatterplot of the maximum enhanced resolution wind speed within a 100 km radius of the interpolated best-track position vs. the best-track maximum sustained (1 min) wind speeds. The mean value at each best-track reported maximum speed is shown with a black square. The diagonal is shown in red, and the gust factor line is shown in green.

50 m/s. We note that the average 100 km radius maximum wind speeds for ultra-high resolution wind fields (black squares in Fig. 4.20) very closely approximate the the gust factor augmented maximum wind speeds for lower NHC speeds. As the NHC maximum sustained wind speed increases, the geophysical model function clipping becomes more influential and the approximation degrades.

Chapter 5

Conclusion

This thesis has evaluated the usefulness of standard and enhanced resolution QuikSCAT wind fields for observation and tracking of tropical cyclones. Observable storm features have been compared. Center fixes have been estimated using standard and enhanced resolution wind fields for all Northern Atlantic and Eastern Pacific tropical cyclones occurring within the SeaWinds-on-QuikSCAT and the SeaWinds-on-ADEOS-II mission lifetimes. These center fixes have been compared with National Hurricane Center (NHC) best-track data to establish a measure of utility for scatterometer wind fields at each resolution.

5.1   Summary of Contributions

A number of contributions to the study of tropical cyclones using space-borne remote sensing have been made. The following sections briefly summarize these contributions.

5.1.1   Utility Demonstration of Resolution-Enhanced Scatterometer Data for Tropical Cyclones

Chapter 3 compared a number of representative tropical cyclone observation conditions in order to differentiate the storm features visible within standard and enhanced resolution QuikSCAT wind fields. The increased resolution in the 2.5 km wind field enables monitoring of the inner core size and structure and the presence of concentric eyewalls. These features are often difficult to distinguish in 25 km wind fields. The enhanced resolution wind fields also permits the observation of storms

79

closer to land than the standard 25 km field. Even in wind fields with rain-induced cross-track pinning of the wind directions, storm structure is manifested in the 2.5 km retrieved wind speeds. We conclude that enhanced resolution QuikSCAT wind fields are useful for observing structural features in tropical cyclones.

Chapter 4 entails an analysis of 2513 tropical cyclone observations by QuikSCAT for the presence of a detectable circulation center in the standard L2B and resolution enhanced wind fields. Circulation centers are detectable in 1512 enhanced resolution observations and in 1298 standard resolution observations. Center fixes obtained from enhanced resolution wind fields are closer to the NHC best-track and achieved with greater analyst confidence than those obtained from standard resolution wind fields. The maximum wind speeds within the enhanced resolution fields more closely match the values reported by the NHC. Additionally, enhanced resolution QuikSCAT observations—especially during the tandem mission time frame—have demonstrated usefulness for monitoring cyclogenesis and tropical cyclone evolution. These results suggests that the increased adoption of enhanced resolution QuikSCAT wind fields may positively impact meteorological and climatological studies relating to tropical cyclones.

5.1.2 Global, Multi-Year Observation Data Set

Pursuant to the analysis of tropical cyclone observation and tracking, a valuable data set of every tropical cyclone observation worldwide by the SeaWinds scatterometers was generated. In total, 6010 storm co-locations are cataloged. The co-location data set includes QuikSCAT rev numbers and georeferencing coordinates for each observation as well as selected NHC best-track reported values. Additionally, ultra-high resolution $\sigma°$ and wind binary data files have been generated for each co-location. From these binary data files, .gif images of standard and enhanced resolution winds and $\sigma°$'s have been generated. Each component of this data set has been made available to the scientific community either by NOAA's QuikSCAT storm page or through the Scatterometer Climate Record Pathfinder at `http://scp.byu.edu`.

5.2 Future Research

Currently, during ambiguity selection for scatterometer wind retrieval, vector winds are nudged by temporally and spatially coarse model wind fields. The location and characterization of cyclonic storms within these model winds is often in error. This error may be partially perpetuated through the final QuikSCAT wind field. The availability of more accurate tropical cyclone center fixes to the ambiguity removal algorithm may improve the nudging field and overall accuracy of retrieved winds.

This thesis has demonstrated the locatability of circulation centers within the QuikSCAT enhanced resolution wind speed field. Since wind ambiguities differ primarily in direction, the presence of a circulation center may be detectable before ambiguity removal. The incorporation of knowledge about tropical cyclone positions into real-time wind retrieval, however, would require an automated computer algorithm to perform the center fix analysis.

As QuikSCAT is known to suffer from rain contamination, a significant component of tropical cyclones, comparison of winds in the co-location set used herein with precipitation data sets from instruments such as the Tropical Rainfall Measuring Mission (TRMM) may yield insight into the nature of this contamination at extremely high rain rates. Additional comparison with QuikSCAT enhanced resolution simultaneous wind/rain retrievals may prove helpful in its validation.

Bibliography

[1] J. Von Ann and J. Sienkiewicz, "The operational impact of QuikSCAT winds at the National Oceanic and Atmospheric Administration Ocean Prediction Center," in *Geoscience and Remote Sensing Symposium, 2004. IGARSS '04. Proceedings*, vol. 5, pp. 3180–3183, IEEE International, 2004.

[2] B. J. Sharp, M. A. Bourassa, and J. J. OBrien, "Early detection of tropical cyclones using SeaWinds-derived vorticity," *Bulletin of the American Meteorological Society*, vol. 83, pp. 879–889, 2002.

[3] R. Atlas, S. C. Bloom, J. Ardizzone, E. Brin, and J. Terry, "Impact of SeaWinds scatterometer data on ocean surface analysis and weather prediction," in *OCEANS 2003. Procedings*, vol. 3, pp. 1698–1601, IEEE International, September 2003.

[4] W. T. Liu, "Progress in scatterometer application," *Journal of Oceanography*, vol. 58, pp. 121–136, 2002.

[5] D. G. Long, "High resolution wind retrieval from SeaWinds," in *Proceedings of the International Geoscience and Remote Sensing Symposium*, (Sydney, Australia), pp. 2187–2189, July 2001.

[6] G. J. Holland, "Global guide to tropical cyclone forecasting," Tech. Rep. WMO/TC-No. 560, TCP-31, World Meteorological Organization; Geneva, Switzerland, 1993.

[7] R. A. Pielke, *The Hurricane*. Routledge, New York, NY, 1990.

[8] NOAA, "Tropical cyclone structure." <http://www.srh.noaa.gov/jetstream /tropics/tc_structure.htm>, October 1, 2006.

[9] T. Lungu, *QuikSCAT Science Data Product User's Manual: Overview and Geophysical Data Products, version 3.0.* Jet Propulsion Lab., Pasadena, Calif., June 2006.

[10] D. G. Long, P. Hardin, and P. T. Whiting, "Resolution enhancement of spaceborne scatterometer data," *IEEE Transactions on Geoscience and Remote Sensing*, vol. 32, no. 3, pp. 700–715, 1993.

[11] M. W. Spencer, C. Wu, and D. G. Long, "Improved resolution backscatter measurements with the SeaWinds pencil-beam scatterometer," *IEEE Transactions on Geoscience and Remote Sensing*, vol. 38, no. 1, pp. 89–104, 2002.

[12] C. Weatherford and W. M. Gray, "Typhoon structure as revealed by aircraft reconnaissance. Part II: Structural variability," *Monthly Weather Review*, vol. 116, pp. 1044–1056, 1988.

[13] K. B. Katsaros, P. W. Vachon, W. T. Lio, and P. G. Black, "Microwave remote sensing of tropical cyclones from space," *J. of Oceanography*, vol. 58, pp. 137–151, 2002.

[14] S. H. Yueh, B. W. Stiles, and W. T. Liu, "QuikSCAT wind retrievals for tropical cyclones," *Geoscience and Remote Sensing, IEEE Transactions on*, vol. 41, pp. 2616–2628, 2003.

[15] D. S. Early and D. G. Long, "Image reconstruction and enhanced resolution imageing from irregular samples," *IEEE Trans. Geosci. Remote Sensing*, vol. 39, pp. 291–302, February 2001.

[16] D. W. Draper and D. G. Long, "Evaluating the effects of rain on SeaWinds scatterometer measurements," *Journal of Geophysical Research*, vol. 109, no. C02005, doi:10.1029/2002JC001741, 2004.

[17] D. W. Draper and D. G. Long, "Simultaneous wind and rain retrieval using SeaWinds data," *IEEE Transactions on Geoscience and Remote Sensing*, vol. 41, no. 7, pp. 1411–1423, 2004.

[18] C. C. Hennon, D. G. Long, and F. J. Wentz, "Validation of quikscat wind retrievals in tropical cyclone environments," in *14th Conference on Satellite Meteorology and Oceanography*, American Meterological Society, 2006.

[19] J. L. Franklin and D. P. Roberts, "Tropical cyclone report Hurricane Lisa 19 September - 3 October 2004," tech. rep., National Hurricane Center, <www.nhc.noaa.gov/2004atlan.shtml>, 10 November 2004.

[20] R. D. Knabb, J. R. Rhome, and D. P. Brown, "Tropical cyclone report Hurricane Katrina 23-30 August 2005," tech. rep., National Hurricane Center, <www.nhc.noaa.gov/2005atlan.shtml>, 20 December 2005.

[21] H. E. Willoughby, J. A. Clos, and M. G. Shoreibah, "Concentric eye walls, secondary wind maxima, and the evolution of the hurricane vortex.," *J. Atmos. Sci*, vol. 39, pp. 395–411, 1982.

[22] J. D. Hawkins and M. Helveston, "Tropical cyclone multiple eyewall characteristics," in *Proceedings of the 26th Conference on Hurricanes and Tropical Meteorology*, 2004.

[23] J. Bevan and H. Cobb, "Tropical cyclone report Hurricane Isabel 6 - 19 September 2003," tech. rep., National Hurricane Center, <www.nhc.noaa.gov/2003atlan.shtml>, 16 January 2004.

[24] J. Bevan and H. D. Cobb, "Tropical cyclone report Hurricane Ophelia 6-17 September 2005," tech. rep., National Hurricane Center, <www.nhc.noaa.gov/2005atlan.shtml>, 14 June 2006.

[25] R. J. Pasch, E. S. Blake, H. D. C. III, and D. P. Roberts, "Tropical cyclone report Hurricane Wilma 15-25 October 2005," tech. rep., National Hurricane Center, <www.nhc.noaa.gov/2005atlan.shtml>, 12 January 2006.

[26] E. S. B. Richard J. Pasch, Daniel P. Brown, "Tropical cyclone report Hurricane Charley 9-14 August 2004," tech. rep., National Hurricane Center, <www.nhc.noaa.gov/2004atlan.shtml>, 5 January 2005.

[27] R. J. Pasch and D. P. Brown, "Tropical cyclone report Hurricane Erin 1-15 September 2001," tech. rep., National Hurricane Center, <www.nhc.noaa.gov/2001.html>, 25 January 2001.

[28] M. D. Powell, P. P. Dodge, and M. L. Black, "The landfall of Hurricane Hugo in the Carolinas: Surface wind distribution," *Weather Forecasting*, vol. 6, pp. 379–399, 1999.

Appendix A

Automated Data Set Processing

This appendix documents the tools and procedure for generating the co-location and center fix data sets for QuikSCAT winds and NHC best-tracks. The procedure is broken down into three principal steps: co-location and image creation, track determination, and visualization. Tools used employ a combination of Perl scripts, Fortran programs, and Matlab functions. They are outlined below.

- Co-location and image creation

  1. PROCESSHRFROMBT.M – Finds co-locations between best-tracks and QuikSCAT revs. Creates Matlab format Rev.mat files for each co-located storm. They are formatted as a struct with the following fields:

     - YEAR: Year (UTC) of QuikSCAT observation
     - JDAY: Day (UTC) within year of observation
     - FILENAME: QuikSCAT L2B HDF filename
     - BESTLAT: NHC best-track latitude spline-interpolated to QuikSCAT observation time
     - BESTLON: NHC best-track longitude spline-interpolated to QuikSCAT observation time
     - MAXSPEED: NHC best-track reported maximum wind speed

  2. CONVERTREVLISTS2TXT.M – Converts the Rev.mat files to .txt file for human readability and data preservation (ASCII instead of .mat). The filename for the text file is set in the Matlab variable <TextFileName>

defined at the beginning of the script. This script could be integrated into processHRFromBT to streamline work flow.

3. QSProcess*HurricaneList.pl – Automates calling of NRT_HiLoRes3.pl for processing enhanced resolution and for creation of .gifs. Uses the .txt file created by ConvertRevLists2Txt for co-location and filename inputs. Can accept regular expressions within the Perl code to select different years, basins, and storms to process. Source and Destination directories are set within the Perl code. Each different QSProcess*HurricaneList.pl file is configured to process a different storm basin. This allows faster processing by simultaneously processing all of the basins.

4. NRT_HiLoRes3.pl – Perl scrips that actually calls the Fortran wind retrieval and image generation programs for processing into HR and .gifs. Flags at beginning of Perl code allow to select which images are created and if they are moved into the final directories or not. For automated processing, this is called by QSProcess*HurricaneList.pl.

- Track determination

1. CreateStormFigs.m – Matlab script that creates Matlab .fig images of storms. Beginning of the .m code allows to select from which basins or years to create figures. This is done as a char array. The destination directory is also set here. Uses the supplementary Matlab function plotHeye6.m for image generation.

2. Heyes3.m – Displays all storm .fig images and prompts for center location input by clicking on the image. Writes one <Storm>DTrack.txt file per storm in the figure directory and copies it to <DerivedTrackDir> (defined at the top of the script). Can select which basins and years to process at the beginning of the .m script.

3. Heye3.m – Called by Heyes3.m to do the actual displaying of the wind fields and returning of the selected center fix lat/lon.

4. COMBINEALLDERIVEDTRACKS.M – Combines all of the individual <Storm>DTrack.txt files in the <DerivedTrackDir> (defined at the beginning of the script) into a single large derived track .txt file called <AllDerivedTrackFileName> (defined at the beginning of the .m script)

5. COMPAREMAXSPEEDS.M – Process <AllDerivedTrackFileName> (defined at the beginning of the .m script) and determines the maximum QuikSCAT (standard and enhanced resolution) wind speed within 50 and 100 km radii of the interpolated best-track position. Outputs a new .txt file similar to <AllDerivedTrackFileName>, but also including the maximum QuikSCAT wind speeds. This filename is defined as <AllDerivedTrack-NewFileName> at the beginning of the .m script

- Visualization

  1. PLOTHEYE8.M – Plots the observation for a given center fix. Input arguments are HRBasin, HRStormYear, HRStormNumber, HRStormName, HRRev, and plotTracks (optional). They are defined as follows:

     – HRBASIN – The tropical cyclone basin of the storm (e.g. 'AL') in single quotes.

     – HRSTORMYEAR – The tropical cyclone season of the storm (e.g. '2002') in single quotes.

     – HRSTORMNUMBER – The two character number of the storm within the season (e.g. '05' not '5') in single quotes.

     – HRSTORMNAME – The name of the cyclone (e.g. 'KATRINA') fully capitalized and in single quotes.